Univerzita Karlova v Praze
Matematicko-fyzikální fakulta

DIPLOMOVÁ PRÁCE

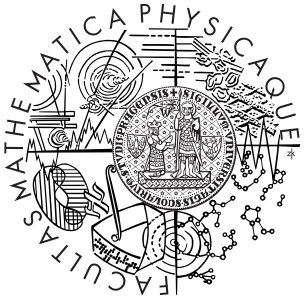

Vjačeslav Sochora

Vliv silného gravitačního pole kompaktních objektů na jejich záření

Astronomický ústav UK

Vedoucí diplomové práce: Doc. RNDr. Vladimír Karas, DrSc.

Studijní program: Fyzika, Astronomie a astrofyzika

2009

Chtěl bych poděkovat svému vedoucímu V. Karasovi za trpělivost, ochotu a za dostatečnou motivaci k dopracování diplomové práce. Chci také poděkovat za jeho připomínky k textu. Dále děkuji T. Pecháčkovi za jeho věcné připomínky a rady ohledně práce. Také děkuji Z. Hrbáčkové za pomoc při sazbě textu a obrázků.

Prohlašuji, že jsem svou diplomovou práci napsal samostatně a výhradně s použitím citovaných pramenů. Souhlasím se zapůjčováním práce a jejím zveřejňováním.

V Praze dne 15.4.2009 Vjačeslav Sochora

Contents

Název práce: Vliv silného gravitačního pole kompaktních objektů na jejich záření
Autor: Vjačeslav Sochora
Katedra (ústav): Astronomický ústav UK
Vedoucí bakalářské práce: Doc. RNDr. Vladimír Karas, DrSc.
e-mail vedoucího: vladimir.karas@cuni.cz

Abstrakt: V předložené práci popisujeme různé vesmírné systémy, které obsahují kompaktní objekty (neutronové hvězdy nebo černé díry). Hlavním zdrojem záření je akrece hmoty na kompaktní objekt, a proto bereme v úvahu několik modelů akrece. Energie emitovaného záření je jiná než pozorovaného. Je to způsobeno gravitačním rudým posuvem a Dopplerovým jevem. Zajímá nás minimální a maximální hodnota této změny emitovaného záření. Ukážeme si, jak spočítat tyto extrémy v Kerrově metrice pomocí eliptických integrálů, jestliže známe emisní poloměr, moment hybnosti černé díry a inklinaci pozorovatele.

Klíčová slova: kompaktní objekty, Kerrova metrika, gravitační rudý posuv

Title: The influence of strong gravity of compact objects on their radiation
Author: Vjačeslav Sochora
Department: Astronomical Institute of Charles University in Prague
Supervisor: Doc. RNDr. Vladimír Karas, DrSc.
Supervisor's e-mail address: vladimir.karas@cuni.cz

Abstract: In the present work we describe different cosmic systems that contain the compact objects (neutron stars or black holes). The accretion of the matter on the compact object is a main source of the radiation and that is why we consider several models of accretion. The energy of emitted radiation is different from the observed energy due to the gravitational redshift and the Doppler shift. We are interested in the minimum and maximum values of this change of emitted radiation. We show how to calculate these extremes in Kerr metric by the help of the elliptic integrals assuming that the emission radius, the angular momentum of black hole, and the inclination angle of the observer are given.

Keywords: compact objects, Kerr metric, gravitational redshift

Chapter 1

Introduction

The main source of the information about the space objects is the electromagnetic radiation from them, namely, the radiation spectrum and its time variability. First, the sky was observed in the visible light. With the development of telescopes we can reach beyond our Solar system, beyond the borders of our Galaxy to the deep space. The visible light showed us the planets in Solar system, the nebulas where new stars are formed, the remnants of the supernovas, and the galaxies. The visible light gives us the information about the morphology of the objects in space.

The cosmic systems do not shine only in the visible light, they radiate also in other wavelength: radio, infra-red, ultra-violet, X-ray and gamma radiation. We can recognize from the type, periodic variations and profiles of the radiation the kind of the object, the ongoing processes, basic parameters (e.g. the mass, the age, the periods, the temperature,...) and many other characteristics of the system. That is why it is important to understand the origin and characteristics of the radiation.

The compact objects and their radiation are main theme of my work. In the following chapter we describe different systems where the compact objects (neutron stars or black holes) are contained and what are their basic properties. In the third chapter we summarize several models that describe the origin of the radiation and what solution they give us.

In fourth chapter we summarize the Kerr metric as a fundamental mathematical framework to describe the null geodesics and to calculate the shift of the frequency of the radiation. If we had an analytic procedure to find the minimum and maximum of the shift (the range of spectral line) then we could more simply find out the parameters of the compact object (the mass and the spin of the black hole).

In the chapters 6-8 we see the results of this work, how the solution looks like and how the minimum and the maximum of the shift depend on these parameters: radius where the emission takes place, inclination angle of the observer and angular momentum of the black hole.

Chapter 2

Compact objects

2.1 The X-ray astronomy

The X-ray astronomy provides the essential information about the physical processes and radiation mechanisms near compact objects (e.g. [7], [30]). The X-rays from the space are completely absorbed by the Earth's atmosphere and that is why the astronomers need to carry out the measuring instruments and to observe the X-ray sky from the space. Among the most important result that the observed data brought was the discovery of X-ray binaries systems. The primary component of this system is a neutron star or a black hole and the companion star usually is a main sequence star. The matter from the companion star accretes onto the compact object via a stellar wind or via Roche lobe overflow. The gravitational potential energy of the accreting matter is converted into an emission radiation from the surface of compact object and from an accretion flow [13] and it is mostly in X-ray range. Accretion stands also behind the energy liberation in the active galactic nuclei. The study of this X-ray emission gives us a useful information about the physics of the accretion and it is a system under physical conditions that are unattainable on the Earth.

The first X-ray source outside the Solar system (in the Solar system it is the Sun) was detected in July 1962, it was the source Sco X-1 in the constellation Scorpio. Another source was discovered in the Crab Nebula in 1964 and the first extragalactic source was M 87 (the figure 2.1). More detailed information are in [15], [10]. On December 12, 1970 NASA launched the famous X-ray satellite UHURU [20]. UHURU discovered about one hundred galactic and fifty extragalactic X-ray sources in the spectral range 2-20 keV in two years. Ones of these source are Hercules X-1 with a short X-ray pulsation with the period of 1.24 s and the source Cyg X-1, a black hole candidate.

In 1975 and 1976 was discovered (using the satellites ANS, SAS-3, OSO 7, 8) a new class of the X-ray sources, so called bursters. Their luminosity rises in a few seconds to 10^{39} erg.s^{-1} and falls back to the original value after about a minute. This repeats from few hours to several days.

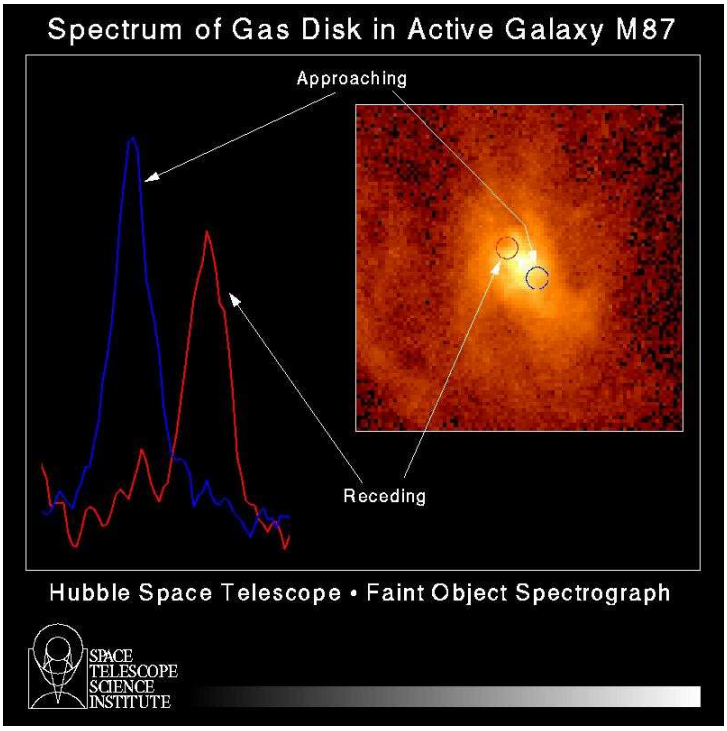

Figure 2.1: Spectrum of gas disk in active galaxy M 87.

The satellite HEAO-2 ([17]) gave us a first look to the central core of the active galaxies, the European satellite EXOSAT discovered a quasi-periodic oscillations in the light curves of X-ray binaries and allowed to understand the nature of X-ray bursts. Another satellites were Japanese Ginga, German ROSAT, NASA's RXTE. The new generation satellites are ESA's XMM and NASA's Chandra.

2.2 Active Galactic Nuclei (AGN)

Active galactic nuclei are objects that have a strong non-thermal nuclear continuum emission and the radiation from their nucleus dominates. Some of them exhibit powerful jets. The nuclear emission lines are not excited by stellar continuum radiation and the nuclear continuum and emission lines are variable. The total luminosity L lies in the range $10^{42} - 10^{47}\text{erg.s}^{-1}$. More information are involved in [24] and [25].

The AGN's are divided into several groups depending on the inclination of the observer:

Radio Galaxies (RGs): The compact source usually lies between two extended radio structures in a form of lobes. The radio emission reaches the distance of $10 - 1000$ kpc. The RGs are divided into two subgroups: *Weak Radio Galaxies (WRGs)* ($L_{1.4\text{GHz}} < 10^{25}\text{W/Hz}$) and *Powerful Radio Galaxies (PRGs)* ($L_{1.4\text{GHz}} > 10^{25}\text{W/Hz}$).

Quasars (QSOs): "quasi-stellar" extragalactic objects (angular size < 1") with broad emissions lines. About 10% quasars are "radio load" ($L_{5\mathrm{GHz}} > 10^{25}$ W/Hz) and the rest "radio quiet".

BL Lac objects: They are strong X-ray sources ($L > 10^{47}$ erg.s^{-1}) and are highly variable in radio, optical and X-ray spectral regions. They have any broad optical emission lines. Optical polarization is strong and variable.

Optically violent variables (OVVs): They are the same as BL Lac objects, but with broad optical emission lines.

Blasars: A unifying term for BL Lac objects, OVVs and highly polarized quasars.

Syefert 1 galaxies (Sy 1): Spiral galaxies with spectra contain permitted emission lines with broad wings and narrower forbidden lines.

Syefert 2 galaxies (Sy 2): Spiral galaxies with equally wide permitted and forbidden lines without broad wings.

Low ionization nuclear emission regions (LINERs): These objects have strong lines of low ionization of some species (O I, S II, etc.).

Nuclear HII regions: Regions of ionized hydrogen in nuclei of many normal inactive galaxies.

Starburst galaxies: Strong IR radiation and they contain young stars. There is a vary intense rate of star formation in these galaxies.

Luminous infrared galaxies: Galaxies luminous in the far infrared region ($L > 10^{45}$ erg.s^{-1}). Intense IR emission may be due to dust radiation which is initiated by an AGN or by intense stellar formation in the galaxy.

2.3 General characteristic and classification of X-ray binaries

Because we have direct observational evidences, we suppose that the compact X-ray sources are the binary systems with a compact object (a neutron star or a black hole) accreting the gas from a nearby, normal companion star and the gravitational potential energy of the gas is converting into X-ray radiation [14], [16], [18]. The evidence is periodic eclipses of the X-ray source by its companion, periodic Doppler shifts of the optical spectral lines of the companion and of the pulsation period of the X-ray source and in some cases heating of one face of the companion star by the X-ray source. Binary periods are typically of the order of days. The most of the X-ray binaries lays in the Galactic plane, we know about 200 binaries [32].

There are two different cases of the transfer of the mass from the primary to the compact secondary in X-ray sources: by Roche or tidal lobe overflow, or by a stellar wind. In the case of Roche (the spin of the primary is synchronized with the binary rotation) or tidal (the primary is not rotating significantly) lobe overflow the primary fills its first equipotential (Roche or tidal lobe) and the material flows slowly from the primary over the gravitational potential saddle point between the two stars (the inner

Lagrangian saddle point L_1) and is quickly captured by the compact object. The mass loss rates are from 3×10^{-8} to $3 \times 10^{-4} M_\odot$ yr^{-1} [12]. The captured plasma forms an accretion disk around the compact star due to the angular momentum.

In the case of the stellar wind the compact object gravitationally captures the ejected plasma from the primary (O or B supergiants), but only a small fraction of the ejected plasma ($\leq 0.1\%$) is captured. The plasma has not sufficient angular momentum to form an accretion disk and the accretion is more or less spherical. The mass loss of the primary star is $10^{-7} - 10^{-6} M_\odot$ yr^{-1} and this leads to the accretion rate $10^{-9} M_\odot$ yr^{-1} [11].

The binaries are divided into two classes [5]: High Mass X-ray Binary (HMXRB) and Low Mass X-ray Binary (LMXRB) depending up the ratio between X-ray $L_{\rm x}$ and optical $L_{\rm opt}$ luminosity

$$\epsilon = \frac{L_{\rm x}(2 - 10{\rm keV})}{L_{\rm opt}(300 - 700{\rm nm})} \tag{2.1}$$

The ratio $\epsilon \leq 10$ is for HMXRB and $\epsilon \gg 10$ for LMXRB. The HMXRBs have a high optical luminosity because the companion star is a early-type massive star (O or B star), while in the LMXRBs the companion star is a low mass star (K-M star or white dwarf) and the optical luminosity is mainly from the accretion disk.

2.4 High Mass X-ray Binaries (HMXRB)

These systems are very young objects ($< 10^7$ years). The companion star is a star of population I and the second star is a neutron star with a strong magnetic field (higher than 10^{12} G), or it is a black hole. The accretion is formed by a strong stellar wind from the companion star. The accretion can also be created by Roche lobe over-flow. The HMXRBs are divided into two groups with respect to the spectral type of their companion: (i) The companion fills its Roche lobe, is of spectral type less than B2 and has evolved off the main sequence. The orbits are circular and the orbital periods are less than 10 days. The mass transfer is mainly via the strong stellar wind. (ii) The companion star is a B-emission (Be) star with emission lines (mainly the Balmer series) that originate in circumstellar material that concentrate in the equatorial plain of the star and is probably due to its rapid rotation. The orbits are eccentric with long periods.

The periods of X-ray pulsations are from 69 ms to 24 min and depend on the geometry of the system [26], [31]. For high luminosities ($\geq 10^{37}$erg.s^{-1}) is the accretion geometry cylindrical; photons escape from the sides of the high density post-shock accretion column. For the lower luminosities ($\leq 10^{37}$erg.s^{-1}) is the infalling material decelerated only above the polar cap. The photons escape from a thin layer on the neutron star surface in the direction of the field line.

Periodic changes are observed in the periodic X-ray pulsation, which reflect spin-up or spin-down of the neutron star. If the inner disk rotates faster than the magnetosphere then the angular momentum is transferred to the neutron star and the pulsar is spined-up. If the inner disk rotates slower than the magnetosphere then the pulsar is spined-down.

The X-ray spectra can be describe by a power law $F(E) = AE^{-\alpha}$, where $F(E)$ is the flux in photons $\mathrm{cm}^{-2}.\mathrm{s}^{-1}$ and the photon index $\alpha \sim 1$. At high energies (15-20 keV) the power law is modified by an exponential cutoff.

Some examples of HMXRBs are Cyg X-1, Cen X-3, 2U 0900-40.

2.5 Low Mass X-ray Binaries (LMXRB)

These objects are very old systems ($> 10^9$ years) without a strong stellar wind. The accretion is formed only if the companion star (of population II) fills its Roche lobe. The neutron star has a weak magnetic filed ($10^8 - 10^9$ G). The optical luminosity of the companion star is much lower than the luminosity of the accretion disk. The orbital periods are in the range from 11 min to 17 days.

In the LMXRB are observed X-ray eclipses, dips, optical brightness variations and type-I or type-II bursts. The eclipses are rare because of the small size of the companion. The dips are sudden decreases of the source intensity, which are probably due to material that accumulates above the disk plane at the point, where the gas stream from the companion hits the accretion disk.

Some examples of LMXRBs are Her X-1, Sco X-1, Cyg X-2, Cyg X-3, GX 17+2.

Of course we don't find only these types of binaries with these properties, we can find single properties of HMXRBs and LMXRBs in one system, e.g. the system can have a star without stellar wind and a compact object with a strong magnetic field, etc. The dividing is only based on the ratio between the luminosities.

Chapter 3

Models of accretion

3.1 The standard model of accretion disks

The standard model of accretion disk describes a thin disk, where the gas moves in an equatorial plane of the cylindrical co-ordinate system [27]. The dynamics of the system is characterized by two conservation equations: mass and angular momentum conservation, respectively the continuity equation and the analogue of the Navier-Stokes equation

$$\frac{\partial \Sigma}{\partial t} + \frac{1}{r}\frac{\partial}{\partial r}(r\Sigma v_r) = 0 \tag{3.1}$$

$$\frac{\partial}{\partial t}(r^2\Sigma\Omega) + \frac{1}{r}\frac{\partial}{\partial r}(r^3\Sigma\Omega v_r) = \frac{1}{2\pi r}\frac{\partial G_{\mathrm{t}}}{\partial r}, \tag{3.2}$$

Here, Ω is an orbital frequency (for a Keplerian disk $\Omega \propto r^{-3/2}$), v_r is the speed in the radial direction, G_{t} is the torque around an annulus and Σ is the one-dimensional surface density due the azimuthal symmetric, $\Sigma(r) = \int \rho(r,z)\mathrm{d}z$, where ρ is the two-dimensional mass density. The nature of the torque is unclear. However, current wisdom points to magnetorotational instability as a likely mechanism [3]. The boundary conditions are different for the binary systems and AGNs. In the first case the mass streams from the companion star by Roche Lobe overflow through the inner Lagrange point or the mass is flushed away by the stellar wind and joins onto the outer edge of the disk. In the AGN's case we have no knowledge of the source of the material forming the disk.

By setting the time derivative of (3.1) to zero we obtain

$$\dot{M} = -2\pi r\Sigma v_r, \tag{3.3}$$

where the $\dot{M}$ presents a gas accreting rate onto a neutron star of mass M_{x} and radius R_{x}. Assume that the accreting gas moves with the freefall velocity v_{ff} and the magnetic field is negligible. When the gas reaches the stellar surface the infall kinetic energy will be converted into heat and radiation. In steady

state, the emergent luminosity $L_{\rm x}$ will be

$$L_{\rm x} = \frac{1}{2}\dot{M}v_{\rm ff}^2 = \frac{G\dot{M}M_{\rm x}}{R_{\rm x}}. \tag{3.4}$$

The efficiency ε of radiative emission is

$$\varepsilon = \frac{L_{\rm x}}{\dot{M}c^2} = \frac{GM_{\rm x}}{R_{\rm x}c^2}, \tag{3.5}$$

where G is the gravitational constant. For typical neutron star it is $\varepsilon \sim 0.1$ (for white dwarf $\varepsilon \sim 3 \times 10^{-4}$, nonrotating black hole $\varepsilon \sim 0.06$, rotating black hole $\varepsilon \sim 0.4$).

If we suppose that the radiation is emitted thermally as blackbody radiation from the surface at temperature $T_{\rm bb}$ then the luminosity $L_{\rm x}$ is

$$L_{\rm x} = 4\pi R_{\rm x}^2 \sigma T_{\rm bb}^4. \tag{3.6}$$

Here, σ is the Stefan-Boltzmann constant. For observed luminosities of 10^{37} erg.s^{-1} the equation gives $T_{\rm bb} \sim 10^7$ K for typical neutron star radii. The accreting neutron stars with this luminosity are natural emitters of X-ray radiation. If we set this luminosity in Eq. (3.4), we obtain the accretion rate $\dot{M} \sim 10^{-9} M_\odot$ yr^{-1}.

Now we define the critical luminosity, so called Eddigton limit, an upper limit to the luminosity of the system. The luminosity depends on the accretion rate $\dot{M}$ and cannot grow ad infinitum. At high luminosities the accretion rate is reduced by the large radiation pressure. The photons emitted by the source interact with the falling matter through processes of scattering and absorption.

Let us compute the upward force $F_{\rm x}$ exerted on infalling matter and the gravitational force $F_{\rm grav}$. The infalling matter is ionized hydrogen and the upward force is due to Thomson scattering off the electrons that then interact with protons by their electrostatic force. Then the upward force $F_{\rm x}$ is at the radius r

$$F_{\rm x} = \frac{L_{\rm x}\sigma_{\rm T}}{4\pi r^2 c}, \tag{3.7}$$

where $\sigma_{\rm T}$ is the Thomson cross section a c the light speed. The gravitational force $F_{\rm grav}$ reacting on protons will be at radius r

$$F_{\rm grav} = \frac{GM_{\rm x}m_{\rm p}}{r^2}. \tag{3.8}$$

Now we will suppose that the forces will be in balance and we obtain then the critical luminosity

$$L_{\rm Edd} = \frac{4\pi c G M_{\rm x} m_{\rm p}}{\sigma_{\rm T}} = 1.3 \times 10^{37} \left(\frac{M_{\rm x}}{M_\odot}\right) {\rm erg.s}^{-1} \tag{3.9}$$

Usually observed luminosities of X-ray binaries are between $0.01L_{\rm Edd}$ and $L_{\rm Edd}$. The scientists observe sometimes the super-Eddington luminosities $L > L_{\rm Edd}$. These can be due to a non steady state accretion, the abundance oh heavy elements or a non-spherical geometry. The Eddington luminosity can also be increased by the presence of a strong magnetic filed

$$\sigma_{\rm mf} = \sigma_{\rm T}\left(\frac{\nu m_{\rm e}}{eB}\right)^2 = 8\times 10^{-3}\sigma_{\rm T}\left(\frac{\nu}{10{\rm keV}}\right)^2\left(\frac{B}{10^{13}{\rm G}}\right)^{-2}, \tag{3.10}$$

where ν is the photon energy and e is an elementary charge. For a magnetic field B of 10^{13} G the Eddington limit is two orders of magnitude higher.

Finally we say the results of the standard model. The first solution is that the radiated energy close to the outer edge of the disk is greater then the gravitational potential energy lost by the gas in the disk. The potential energy from the inner regions is transported out with the angular momentum and is radiated at larger radii. The second solution is that in entire disk is half of the gravitational potential energy radiated away from the disk and the rest of this energy is converted into kinetic energy of the gas.

3.2 The collisionless spherical accretion

In this section we describe a collisionless spherical accretion of identical particles of mass m finding themselves in a collisionless gas [33]. The accretion is onto a central star of mass M and radius R. The particle distribution function $f(\mathbf{r},\mathbf{v},t)$ contains all information about the accretion gas. The definition $f(\mathbf{r},\mathbf{v},t){\rm d}^3t{\rm d}^3v$ determines the number of particles in the phase space volume element ${\rm d}^3t{\rm d}^3v$ centered about $\mathbf{r}$ and $\mathbf{v}$, at time t.

Next we define the particle number density

$$n(\mathbf{r},t) = \int f(\mathbf{r},\mathbf{v},t){\rm d}^3v \tag{3.11}$$

and the velocity dispersion

$$\langle v^2(\mathbf{r},t)\rangle = \frac{1}{n(\mathbf{r},t)}\int v^2 f(\mathbf{r},\mathbf{v},t){\rm d}^3v. \tag{3.12}$$

We can calculate the particle distribution function from the collisionless Boltzmann equation or Vlasov equation

$$\frac{\rm d}{{\rm d}t}f(\mathbf{r},\mathbf{v},t) = \frac{\partial f}{\partial t} + \mathbf{v}.\nabla_{\mathbf{r}}f + \dot{\mathbf{v}}.\nabla_{\mathbf{v}}f, \tag{3.13}$$

where $\mathbf{v} = \dot{\mathbf{r}}$ is the particle velocity along the coordinates $\mathbf{r}$ and $\dot{\mathbf{v}}$ is the acceleration

$$\dot{\mathbf{v}} = -\nabla\Phi, \tag{3.14}$$

where Φ is the gravitational potential

$$\Phi = -\frac{GM}{r} + \Phi_{\rm self}, \tag{3.15}$$

where r is the distance to central star. Hereafter we will ignore the self-gravity term $\Phi_{\rm self}$.

The distribution function f is a function only of the dynamical constants of motion if the flow is stationary and function f is independent of time. Extra for the spherical systems are only two constants of motion: the energy E and the angular momentum J per unit mass, defined by

$$E = \frac{1}{2}v^2 + \Phi(r) = \frac{1}{2}v_{\rm r}^2 + \frac{1}{2}v_{\rm t}^2 - \frac{GM}{r} = \frac{1}{2}v_{\rm r}^2 + \frac{1}{2}\frac{J^2}{r^2} - \frac{GM}{r}, \tag{3.16}$$

$$J = rv_{\rm t}, \tag{3.17}$$

where $v_{\rm r}$ is radial and $v_{\rm t}$ is transverse particles velocities. Specially for the isotropic velocity distribution the distribution function f is independent of J and the function f is a function only of energy E, $f = f(E)$.

In this case the particle number density n (3.11) reduces to

$$n(r) = 4\pi \int v^2 f {\rm d}v = 4\pi \int\limits_{E=\Phi}^{\infty} [2(E-\Phi)]^{1/2} f(E) {\rm d}E \tag{3.18}$$

and the velocity dispersion (3.12) to

$$\langle v^2(r) \rangle = \frac{4\pi}{n(r)} \int\limits_{E=\Phi}^{\infty} [2(E-\Phi)]^{3/2} f(E) {\rm d}E. \tag{3.19}$$

The moving particles with a critical value of angular momentum $J_{\rm min}(E)$ or less will be captured by the central star. For nonrelativistic particles orbiting a Newtonian star of radius R it is

$$J_{\rm min}(E) = \left[2\left(E + \frac{GM}{R}\right)\right]^{1/2} \tag{3.20}$$

and for nonrelativistic particles orbiting a compact object it is

$$J_{\rm min}(E) = \frac{4GM}{c}. \tag{3.21}$$

The total rate of captured particles onto central mass is

$$\dot{N}_{\rm tot} = 8\pi^2 \int\limits_{\Phi(R)}^{\infty} \int\limits_{0}^{J_{\rm min}(E)} f J {\rm d}J {\rm d}E \tag{3.22}$$

and we calculate the mass rate as $\dot{M}_{\rm tot} = m\dot{N}_{\rm tot}$.

If we assume the unbound nonrelativistic particles with energies $E > 0$ then the rate $\dot{N}$ is

$$\dot{N}(E>0) = 4\pi^2 \int\limits_{0}^{\infty} f(E) J_{\rm min}^2(E) {\rm d}E \tag{3.23}$$

and the rate $\dot{M}(E > 0) = m\dot{N}(E > 0)$ for nonrelativistic particles and Newtonian star is

$$\dot{M}(E > 0) = 2\pi G M^2 \rho_\infty v_\infty^{-1} \frac{R}{M} \left(1 + \frac{v_\infty^2 R}{2MG}\right) \tag{3.24}$$

and for a compact star when $(Rc^2)/(GM) < 8$

$$\dot{M}(E > 0) = 16\pi (GM)^2 \rho_\infty v_\infty^{-1} c^{-2} \tag{3.25}$$

or

$$\dot{M}(E > 0) = 1.56 \times 10^{-23} \left(\frac{\rho_\infty}{10^{-24}\mathrm{g.cm}^{-3}}\right) \left(\frac{M}{M_\odot}\right)^2 \left(\frac{v_\infty}{10\mathrm{km.s}^{-1}}\right)^{-1} M_\odot \mathrm{yr}^{-1}, \tag{3.26}$$

where $\rho_\infty = mn_\infty$, $v_\infty \ll c$ and their values are at infinity.

From equations (3.18) and (3.19) when $E > 0$ yields

$$n_{E>0}(r) = n_\infty \left(1 + \frac{2GM}{v_\infty^2 r}\right)^{1/2} \tag{3.27}$$

and

$$\langle v^2(r) \rangle_{E>0} = v^2(r) = v_\infty^2 \left(1 + \frac{2GM}{v_\infty^2 r}\right). \tag{3.28}$$

We furthermore define the particle temperature

$$T_{E>0}(r) = T_\infty \left(1 + \frac{2GM}{v_\infty^2 r}\right) \tag{3.29}$$

and the accretion radius (the kinetic energy of particle is equal to its potential energy)

$$r_\mathrm{a} = \frac{2GM}{v_\infty^2}. \tag{3.30}$$

These last equations describe sufficiently the colisionless spherical accretion, more detailed information are in [28].

3.3 The hydrodynamic spherical accretion

The hydrodynamic view of the spherical accretion is a natural way to describe the flow of particles onto compact objects, because there is an interaction between the particles.

Assume steady, spherical accretion of a gas onto a stationary, nonrotating black hole of mass M, the gas flow is in the first approximation adiabatic and the entropy loss due the radiation as a small perturbation. Define the pressure as

$$P = K\rho^\Gamma, \tag{3.31}$$

where K is a constant and $\Gamma = \text{const.}$ is an adiabatic index characterizing the gas. The sound speed a is given by

$$a = \sqrt{\frac{\mathrm{d}P}{\mathrm{d}\rho}} = \sqrt{\frac{\Gamma P}{\rho}}. \tag{3.32}$$

The gas has at infinity the density ρ_∞, the pressure P_∞ and the sound speed a_∞.

The flow is completely describe by two equations: the continuity equation

$$\nabla.\rho\mathbf{u} = \frac{1}{r^2}\frac{\mathrm{d}}{\mathrm{d}r}(r^2\rho u) = 0 \tag{3.33}$$

and the Euler equation

$$u\frac{\mathrm{d}u}{\mathrm{d}r} = -\frac{1}{\rho}\frac{\mathrm{d}P}{\mathrm{d}r} - \frac{GM}{r^2}, \tag{3.34}$$

where u is the inward radial velocity ($u > 0$).

Integrating the continuity equation (3.33) we obtain accretion rate $\dot{M}$

$$4\pi r^2\rho u = \dot{M} = \text{const.} \tag{3.35}$$

Define the critical or the transonic radius r_s as the radius where the flow speed equals the sound speed

$$r_\mathrm{s} = \left(\frac{5-3\Gamma}{4}\right)\frac{GM}{a_\infty^2} \tag{3.36}$$

and the sound speed at the transonic radius r_s is

$$a_\mathrm{s}^2 = \frac{1}{2}\frac{GM}{r_\mathrm{s}} = \left(\frac{2}{5-3\Gamma}\right)a_\infty^2. \tag{3.37}$$

Institute the equation

$$\rho = \rho_\infty\left(\frac{a}{a_\infty}\right)^{\frac{2}{\Gamma-1}} \tag{3.38}$$

to the equation (3.35) we obtain

$$\dot{M} = 4\pi\rho_\infty a_\mathrm{s} r_\mathrm{s}^2\left(\frac{a}{a_\infty}\right)^{\frac{2}{\Gamma-1}} = 4\pi\lambda_\mathrm{s}\left(\frac{GM}{a_\infty^2}\right)^2\rho_\infty a_\infty, \tag{3.39}$$

where

$$\lambda_\mathrm{s} = \left(\frac{1}{2}\right)^{\frac{\Gamma+1}{2(\Gamma-1)}}\left(\frac{5-3\Gamma}{4}\right)^{-\frac{5-3\Gamma}{2(\Gamma-1)}}. \tag{3.40}$$

We can rewrite the equation (3.39) to the form

$$\dot{M} = 4\pi\lambda_\mathrm{s}(GM)^2\rho_\infty a_\infty^{-1}c^{-2}\frac{c^2}{a_\infty^2} \tag{3.41}$$

and compare with the equation (3.25). We see that the hydrodynamical accretion is larger than the collisionless accretion by the factor c^2/a_∞^2 ($\sim 10^9$ for typical ionized interstellar gas with $a_\infty \sim 10$ km.s^{-1}).

Assume a pure hydrogen with $\Gamma = 5/3$ then the accretion rate is

$$\dot{M} = 8.77 \times 10^{-16} \left(\frac{\rho_\infty}{10^{-24}\mathrm{g.cm}^{-3}}\right) \left(\frac{M}{M_\odot}\right)^2 \left(\frac{a_\infty}{10\mathrm{km.s}^{-1}}\right)^{-3} M_\odot \mathrm{yr}^{-1}. \quad (3.42)$$

The boundary conditions at infinity $u = 0$, $a = a_\infty$, $\rho = \rho_\infty$ for the equations (3.33) and (3.34) give us two solutions: subsonic $\lambda < \lambda_\mathrm{s}$ and transonic $\lambda = \lambda_s$. For a star with hard surface (white dwarf or neutron star) is the flow subsonic and for black holes is the flow transonic.

Finally there is question how large is the luminosity of radiation from spherical accretion onto nonrotating black holes? Assume that the black hole is at rest in a uniform ionized gas of pure hydrogen which has at infinity density $n_\infty \sim 1$ cm^{-3} and temperature $T_\infty \sim 10^4$ K. The dominant mechanism are thermal bremsstrahlung and free-free emission. Then the careful relativistic integration gives the luminosity

$$L_\mathrm{ff} = 1.2 \times 10^{21} \left(\frac{n_\infty}{1\mathrm{cm}^{-3}}\right)^2 \left(\frac{T_\infty}{10^4\mathrm{K}}\right)^{-3} \left(\frac{M}{M_\odot}\right)^3 \mathrm{erg.s}^{-1}. \quad (3.43)$$

This emission corresponds to the radiation of very hard X-rays and γ-rays.

Now we calculate the efficiency of this emission

$$\varepsilon = \frac{L_\mathrm{ff}}{\dot{M}c^2} \sim 6 \times 10^{-11} \left(\frac{n_\infty}{1\mathrm{cm}^{-3}}\right) \left(\frac{T_\infty}{10^4\mathrm{K}}\right)^{-3/2} \left(\frac{M}{M_\odot}\right). \quad (3.44)$$

The efficiency for maximally rotating black hole will increase by 15% above. The spherical accretion onto black holes is an inefficient in contrast to the spherical accretion onto neutron star ($\varepsilon \sim 0.1$) or to the disk accretion onto black hole $\varepsilon \sim 0.05 - 0.42$ that depends on the value of the angular momentum and the direction of the gas relative to the hole, more detailed information are in [28].

The standard thin disk and the hydrodynamical spherical accretion represent just two limiting cases. They capture the most basic features of the accretion process. However there are circumstances when the assumptions of both these approximations are not valid, and then more complicated accretion models may occur: slim disk [2], advection dominated accretion flows [23].

3.4 The interaction of an accretion matter with a magnetic field

As we have seen, most of neutron stars have a strong magnetic field that can interact with the accreting matter. If we assume that the magnetic

field has bipolar structure then the magnetic pressure becomes larger when the matter approaches the neutron star. At a specific radius the magnetic pressure becomes dominant over the ram pressure of the infalling matter and then the magnetic field forces the charged particles flow along magnetic lines. This radius is called Alfvén radius r_{A}.

Most of the emitted luminosity comes from the accretion columns formed above magnetic poles. The magnetic axis usually is inclined with respect to the rotation axis and that's why the observer sees the emission from the accretion column only when the magnetic axis meets the line of his sight. This is the origin of pulsations visible in the spectral lines of highly magnetized compact objects. The pulsation gives us the information about the spin of the compact object. The angular momentum of the accretion matter is transferred to the compact object and changes the spin of the neutron star. This variation of period can be measured and it gives information about the accretion flow.

Chapter 4

Photon propagation in Kerr metric

4.1 Definition and properties of Kerr metric

The Kerr metric ([21], [9]) is both stationary and axisymmetric and describes the gravitational field of the rotating black hole and depends only on two parameters, the mass M of the black hole and its angular momentum per unit mass $a = J/M$. The form of the Kerr metric in Boyer-Lindquist coordinates (t, r, θ, ϕ) $(c = G = 1)$ is

$$\mathrm{d}s^2 = -\Sigma\frac{\Delta}{A}\mathrm{d}t^2 + \frac{A}{\Sigma}\left(\mathrm{d}\phi - \frac{2ar}{A}\mathrm{d}t\right)^2 \sin^2\theta + \frac{\Sigma}{\Delta}\mathrm{d}r^2 + \Sigma\mathrm{d}\theta^2 \tag{4.1}$$

or another form

$$ds^2 = -\left(1 - \frac{2r}{\Sigma}\right)\mathrm{d}t^2 - \frac{4ar}{\Sigma}\sin^2\theta\mathrm{d}t\mathrm{d}\phi + \frac{A}{\Sigma}\sin^2\theta\mathrm{d}\phi^2 + \frac{\Sigma}{\Delta}\mathrm{d}r^2 + \Sigma\mathrm{d}\theta^2, \tag{4.2}$$

where

$$\Sigma = r^2 + a^2\cos^2\theta, \tag{4.3}$$

$$\Delta = r^2 - 2r + a^2, \tag{4.4}$$

$$A = (r^2 + a^2)^2 - a^2\Delta\sin^2\theta, \tag{4.5}$$

where we set $M = 1$ without the lose of generality.

For the case $a = 0$ the Kerr metric corresponds to a nonrotating black hole that is described by Schwarzschild metric

$$\mathrm{d}s^2 = -\left(1 - \frac{2}{r}\right)\mathrm{d}t^2 + \left(1 - \frac{2}{r}\right)^{-1}\mathrm{d}r^2 - r^2(\mathrm{d}\theta^2 + \sin^2\theta\mathrm{d}\phi^2). \tag{4.6}$$

and the solutions for a rotating black hole are only if $a \leq 1$.

The horizons are roots of the equation $\Delta = 0$, the outer and inner horizons:

$$r_\mathrm{h} = r_+ = 1 + \sqrt{1 - a^2}, \tag{4.7}$$

$$r_- = 1 - \sqrt{1 - a^2}. \tag{4.8}$$

The limiting values are $r_\mathrm{h} = 2$ and $r_- = 0$ for $a = 0$ and $r_\mathrm{h} = 1$ and $r_- = 1$ for $a = 1$ (maximally rotating black hole). In the Schwarzschild metric the event horizon is identical to the stationary surface, $g_{tt} = 0$, while in the Kerr metric the stationary surface r_s is described by another equation than the horizon r_h

$$r_\mathrm{s} = 1 - \sqrt{1 - a^2 \cos^2 \theta}. \tag{4.9}$$

The stationary surface is called the static limit and the region $r_\mathrm{h} < r \leq r_\mathrm{s}$ the ergosphere.

The minimum allowed radius of a stable circular equatorial orbit, so called marginally stable orbit, is given by the roots of the equation

$$r^2 - 6r \mp 8a\sqrt{r} - 3a^2 = 0. \tag{4.10}$$

The roots are

$$r_\mathrm{ms} = 3 + Z_2 \mp [(3 - Z_1)(3 + Z_1 + 2Z_2)]^{1/2}, \tag{4.11}$$

where

$$Z_1 = 1 + (1 - a^2)^{1/3}[(1 + a)^{1/3} + (1 - a)^{1/3}], \tag{4.12}$$

$$Z_2 = (3a^2 + Z_1^2)^{1/2}, \tag{4.13}$$

where the upper sign refers to co-rotating and the lower to counter-rotating orbits.

4.2 Null geodesics in Kerr metric

The path of photons (null geodesic) is completely described by three constants of motion, the total energy E, the azimuthal angular momentum L_z and Carter constant Q. We reduce the number of constants by re-normalizing L_z and Q with respect to energy E

$$\lambda = \frac{L_z}{E}, \tag{4.14}$$

$$q^2 = \frac{Q}{E^2}. \tag{4.15}$$

Next the null geodesic must satisfy the Carter equation [8]

$$\pm \int_r \frac{\mathrm{d}r}{\sqrt{R(r, \lambda, q^2)}} = \pm \int_\theta \frac{\mathrm{d}\theta}{\sqrt{\Theta(\theta, \lambda, q^2)}}, \tag{4.16}$$

where

$$R(r) = r^4 + (a^2 - \lambda^2 - q^2)r^2 + 2[q^2 + (\lambda - a)^2]r - a^2 q^2 \tag{4.17}$$

and

$$\Theta(\theta, \lambda, q^2) = q^2 + (a\cos\theta)^2 - (\lambda\cot\theta)^2. \tag{4.18}$$

Suppose the substitution $\mu = \cos\Theta$, then we can rewrite the equation (4.16) to the form

$$\pm\int_r \frac{\mathrm{d}r}{\sqrt{R(r,\lambda,q^2)}} = \pm\int_\mu \frac{\mathrm{d}\mu}{\sqrt{\Theta(\mu,\lambda,q^2)}}, \tag{4.19}$$

where

$$\Theta(\mu, \lambda, q^2) = q^2 + (a^2 - \lambda^2 - q^2)\mu^2 - a^2\mu^4. \tag{4.20}$$

The roots of $R(r)$ and $\Theta(\mu)$ correspond to the turning points in radial and latitudinal direction.

4.3 The roots of $R(r)$

The expression in the equation (4.17) is a polynomial of fourth order and that's why we can write it in the form $R = (r - r_1)(r - r_2)(r - r_3)(r - r_4)$, where r_1, r_2, r_3, r_4 are the roots of $R(r) = 0$. Before writing the roots in the explicit form we define six expressions

$$A = (a^2 - \lambda^2 - q^2), \tag{4.21}$$

$$B = (a - \lambda)^2 + q^2, \tag{4.22}$$

$$C = A^2 - 12a^2q^2, \tag{4.23}$$

$$D = 2A^3 + 72a^2q^2A + 108B^2, \tag{4.24}$$

$$E = \frac{1}{3}\left[\left(\frac{D - \sqrt{-4C^3 + D^2}}{2}\right)^{\frac{1}{3}} + \left(\frac{D + \sqrt{-4C^3 + D^2}}{2}\right)^{\frac{1}{3}}\right], \tag{4.25}$$

$$F = \sqrt{-\frac{2}{3}A + E} \tag{4.26}$$

and

$$D\pm = -\frac{4}{3}A - E \pm \frac{4B}{F}. \tag{4.27}$$

Now we can write the roots of $R(r) = 0$

$$r_1 = \frac{1}{2}F + \frac{1}{2}\sqrt{D_-}, \tag{4.28}$$

$$r_2 = \frac{1}{2}F - \frac{1}{2}\sqrt{D_-}, \tag{4.29}$$

$$r_3 = -\frac{1}{2}F + \frac{1}{2}\sqrt{D_+}, \tag{4.30}$$

$$r_4 = -\frac{1}{2}F - \frac{1}{2}\sqrt{D_+}. \tag{4.31}$$

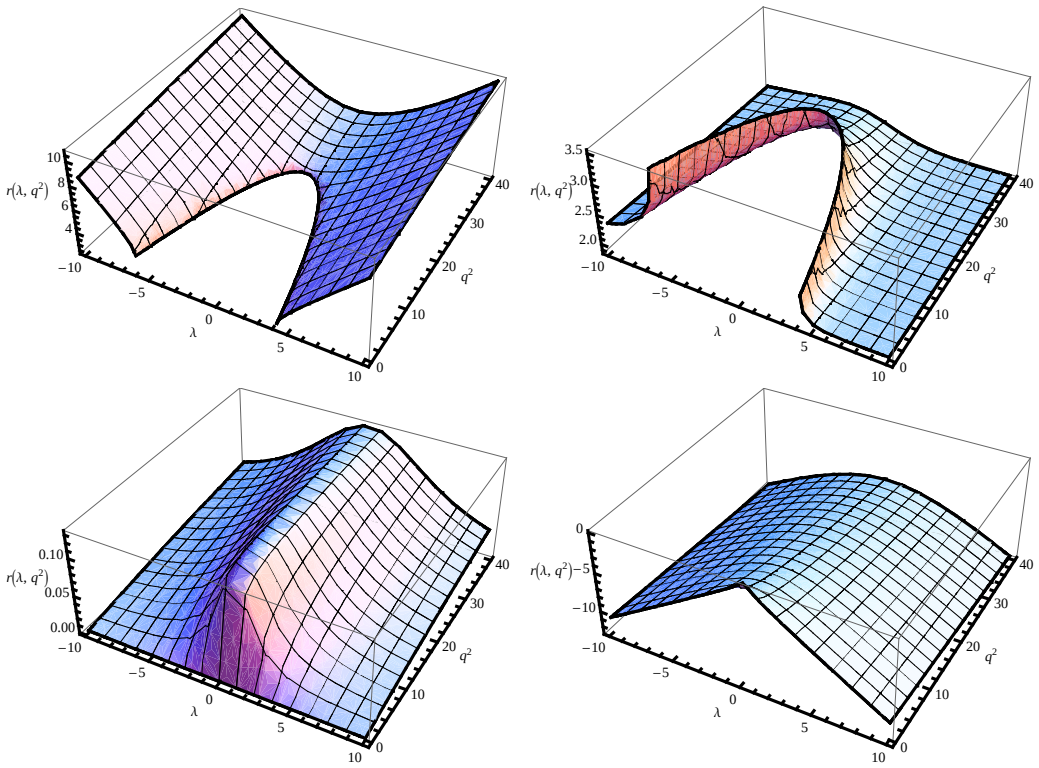

Figure 4.1: The roots $r_1(\lambda, q^2)$ (top left), $r_2(\lambda, q^2)$ (top right), $r_2(\lambda, q^2)$ (bottom left), $r_2(\lambda, q^2)$ (bottom right). All cases are shown for $a = 0.5$.

The roots r_1 and r_2 can be real or complex, while the roots r_3 and r_4 are always real. $r_1 > r_2 > r_3 > r_4$ if the roots are real. The figure 4.1 shows the behavior of the roots for $a = 0.5$. We see that r_4 is always lower than zero and the value of r_3 is lower than the value of horizon event (equation (4.7)), so they have no physical significance. Also we see that the roots r_1 and r_2 are not real for some pairs (λ, q^2), but instead they are complex for these pairs. Physically the roots r_1 and r_2 are the turning points of the null geodesics.

4.4 The roots of $\Theta(\mu)$

The expression in the equation (4.20) can be rewritten as $\Theta(\mu) = a^2(\mu_-^2 + \mu^2)(\mu_+^2 - \mu^2)$, $q^2 > 0$, where the roots are

$$\mu_+^2 = \frac{1}{2a^2}\{[(\lambda^2 + q^2 - a^2)^2 + 4a^2q^2]^{1/2} - (\lambda^2 + q^2 - a^2)\}, \tag{4.32}$$

$$\mu_-^2 = \frac{1}{2a^2}\{[(\lambda^2 + q^2 - a^2)^2 + 4a^2q^2]^{1/2} + (\lambda^2 + q^2 - a^2)\}. \tag{4.33}$$

The roots are for $q^2 > 0$ because all null geodesics that come through the

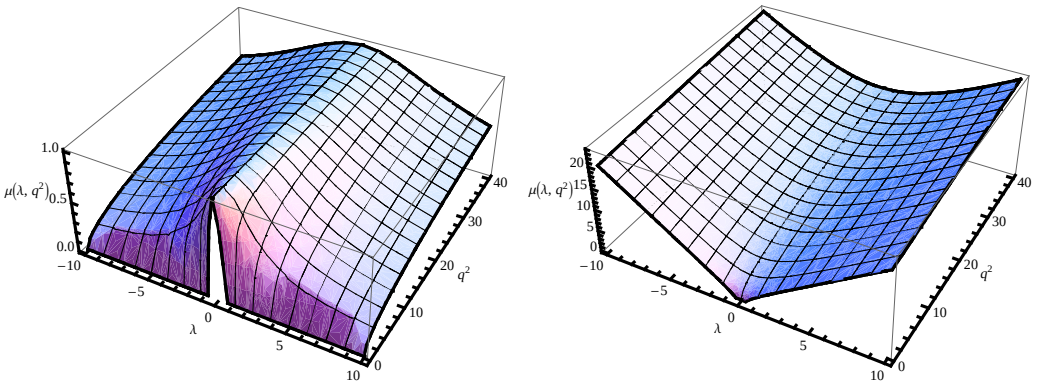

Figure 4.2: The roots $\mu_+(\lambda, q^2)$ (left), $\mu_-(\lambda, q^2)$ (right). All cases are shown for $a = 0.5$.

equatorial plane must satisfy this condition and in the following chapters we assume these null geodesics.

The behavior of the roots is in the figure 4.2. One root takes always the values in range (0-1) and physically is the turning point in the latitudinal direction. The second one has no physically significance for us.

Chapter 5

Photon energy shifts in Kerr metric

5.1 The motivation and the goals

Relativistic iron line profiles provide a powerful tool to measure the mass of the black hole, both in active galactic nuclei and Galactic black hole candidates. They will also help to constrain the black hole spin once the quality of data improves with future detectors. Stella [29] proposed the use of temporal changes in the line profile following variations of the illuminating primary source. Matt & Perola [22] proposed to employ, instead, variations of the integrated line properties (equivalent width, centroid energy and linewidth). Temporal variations of the flux and spectrum, caused by an orbiting spot or a spiral wave, were also examined by various authors (see e.g. [19] for a review). These methods are conceptually similar to the so called reverberation mapping method, widely applied to optical broad lines in AGNs, however, they have not yet provided many results in X-rays. This situation would be highly desirable to improve because most of X-ray signal originates from the inner regions of the accretion disc. This should change with future detectors equipped with high collecting area. Then it will be most relevant to know the expected energy range of iron line profiles, depending on the basic model parameters - i.e., radius where the emission takes place, inclination angle of the observer, and angular momentum of the black hole.

So our goal is to find a formula, where the input parameters would be emission radius, inclination angle of the observer at infinity, and angular momentum of the black hole, and the output would be minimum value and maximum value of the change of the frequency of the radiation from the surround of black hole. We use the Carter equation (which is a condition that the null geodesics must satisfy) in the form of the elliptic integrals to find out the searched formula.

If we find such formula then we could calculate retroactively the parameters of black hole from the knowledge of the observer's position.

5.2 The model

We will suppose the following model of a radiating ring with known radius (e.g., $r_e = r_{\rm ms}, 6, 8, 10$). The ring rotates in the equatorial plane ($\theta_e = \pi/2$) with the angular velocity

$$\Omega = \frac{1}{\sqrt{r_e^3} + a}, \tag{5.1}$$

where $a \in (0, 1)$ is the specific angular momentum of the black hole and the ring radiates isotropically in its co-rotating frame. The photons come from the ring to the observer located at infinity with the inclination angle $\theta_o \in \left(0, \frac{\pi}{2}\right)$.

5.3 The ratio g between $\nu_{\rm obs}$ and $\nu_{\rm em}$

The change of the emitting frequency $\nu_{\rm em}$ is describe as the ratio g between the emitting frequency and the observed frequency $\nu_{\rm obs}$

$$g = \frac{\nu_{\rm obs}}{\nu_{\rm em}}. \tag{5.2}$$

We assume an emitting particle in Kerr metric. The four-velocity of this source is $\mathbf{u} = u^t(1, 0, 0, \Omega)$ where

$$u^t = \left[1 - \frac{2r_{\rm e}}{\Sigma}(1 - a\Omega \sin^2\theta_{\rm e})^2 - (r_{\rm e}^2 + a^2)\Omega^2 \sin^2\theta_{\rm e}\right]^{-1/2} \tag{5.3}$$

and Ω is angular velocity of the particle. The observer is assumed to be located at rest at infinity. Then the ratio g can be expressed as

$$g = \frac{1}{u^t}\frac{1}{1 - \lambda\Omega}. \tag{5.4}$$

It is interesting to show how the function g depends on λ, where the values of function are in the interval $(0, 2.0)$. The behavior is shown in the figure 5.1 for $a = 0.5$, and in figure 5.2 for extreme a, there is no minimum or maximum of the function $g(\lambda)$, but we observe that the width of the spectral line is finite and that's why there must be minimum and maximum value of the change of the frequency. To find them we need a condition for the constant of motion λ that would give us all λ that would correspond to null geodesics coming to the observer at infinite. This condition is the Carter equation (4.16) or (4.19). If we find such values λ (or pairs λ, q^2) then the minimum value of $\lambda_{\rm min}$ will correspond to the minimum value of $g_{\rm min}(\lambda_{\rm min})$ and the maximum value of $\lambda_{\rm max}$ will correspond to the maximum value of the $g_{\rm max}(\lambda_{\rm max})$ (because the function $g(\lambda)$ is monotonously increasing on $g(\lambda) \in (\infty, \Omega^{-1})$).

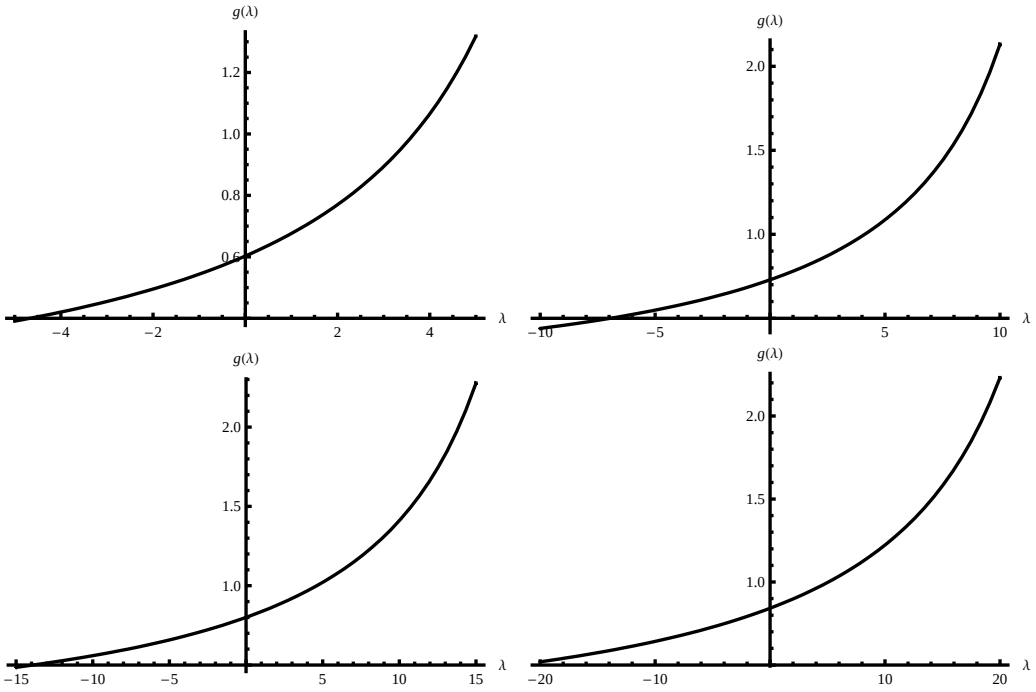

Figure 5.1: The function $g(\lambda)$ for $r_{\rm e} = r_{\rm ms}(= 4.233)$ (top left), $r_{\rm e} = 6$ (top right), $r_{\rm e} = 8$ (bottom left) and $r_{\rm e} = 10$ (bottom right). In all cases $a = 0.5$.

5.4 Definition scope of (λ, q^2)

Before we write the solutions for the r-integral and θ-integral, we make discussions about the turning points in the radial and latitudinal directions: where they are complex, for which (λ, q^2) the null geodesics go to the observer and for which not, etc.

The null geodesic in the radial direction has two turning points r_1, r_2 if the roots are real, or has no one if they are complex. We can see in the figure 4.1 that the turning point r_1 takes the values larger than the radius $r_{\rm e}$ of the ring for some (λ, q^2). In this case the null geodesics can not reach the infinity. Hence, only the null geodesics with the pairs (λ, q^2), for which $r_1 < r_{\rm e}$, can reach the infinity in the radial direction. These pairs are shown in the figures 5.3 and 5.4 for different cases. If we suppose complex r_1, r_2 then we have no problem because these values have not physical sense and the null geodesics can reach the observer in the radial direction.

The area, where the roots are complex, shifts to the negative values of λ with increasing specific angular momentum a of the black hole. It is evident because λ represents the azimuthal angular momentum of the ring particles. In the case that the emitting radius $r_{\rm e}$ is larger than $r_{\rm e} = r_{\rm ms}$, e.g. $r_{\rm e} = 6, 8, 10$, then the area of the possible null geodesics is bigger.

The number of pairs (λ, q^2) that correspond to the null geodesics that reach the observer in the latitudinal direction depends on the inclination of

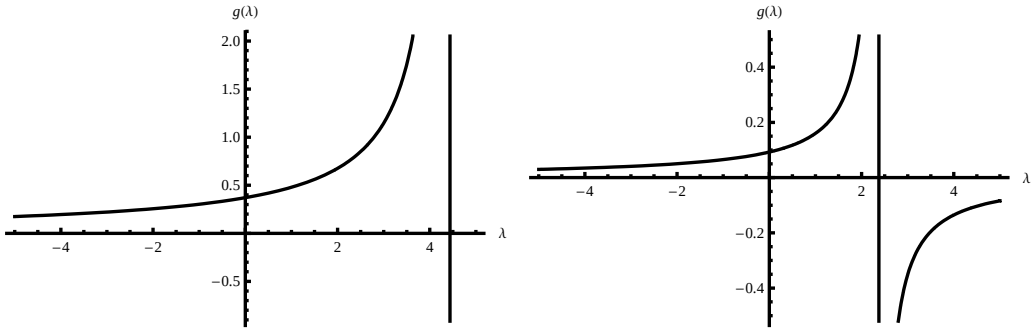

Figure 5.2: The function $g(\lambda)$ for $a = 0.9$ (left) and $a = 0.998$ (right) when $r_{\mathrm{e}} = r_{\mathrm{ms}}$.

the observer. This dependence is shown in the figure 5.5. If the inclination is small then there is a small area of (λ, q^2) which correspond to the null geodesics that reach the observer in latitudinal direction. If the inclination is greater then the area is larger.

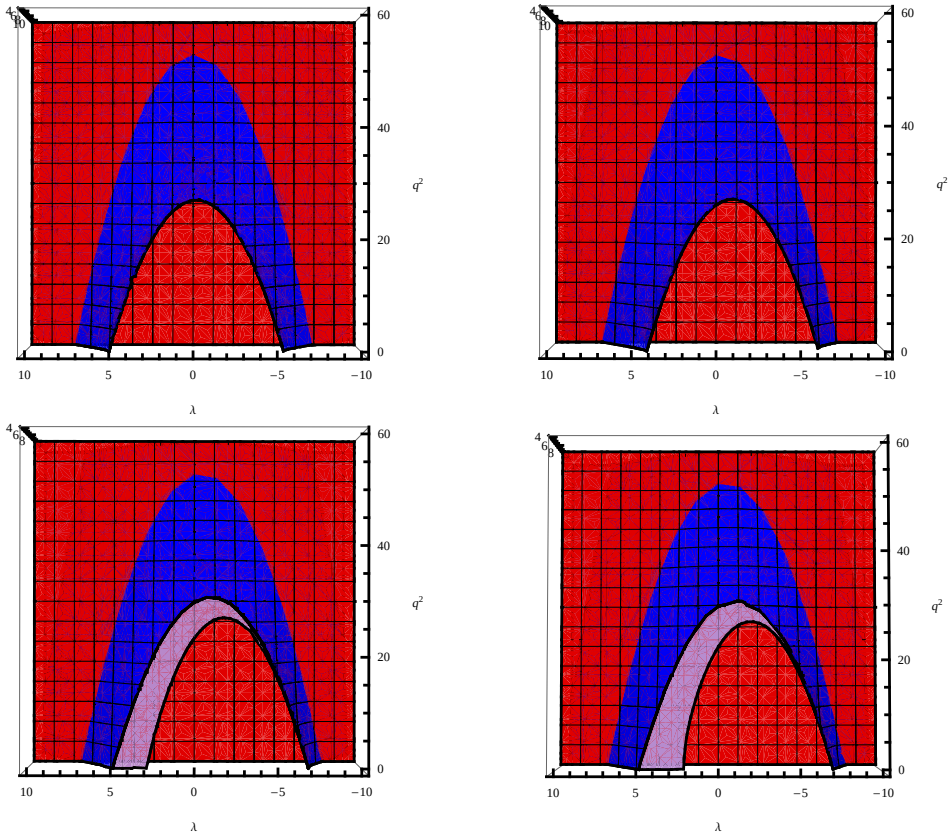

Figure 5.3: The outer red area represents null geodesics that don't reach the observer, whereas the inner red area represents null geodesics with complex turning points and the blue (and violet) area represents possible null geodesics that reach the observer in the radial direction. The emission radius is $r_{\rm e} = 6$ and it is shown for the cases $a = 0.1$ (top left), $a = 0.5$ (top right), $a = 0.9$ (bottom left), $a = 0.998$ (bottom right).

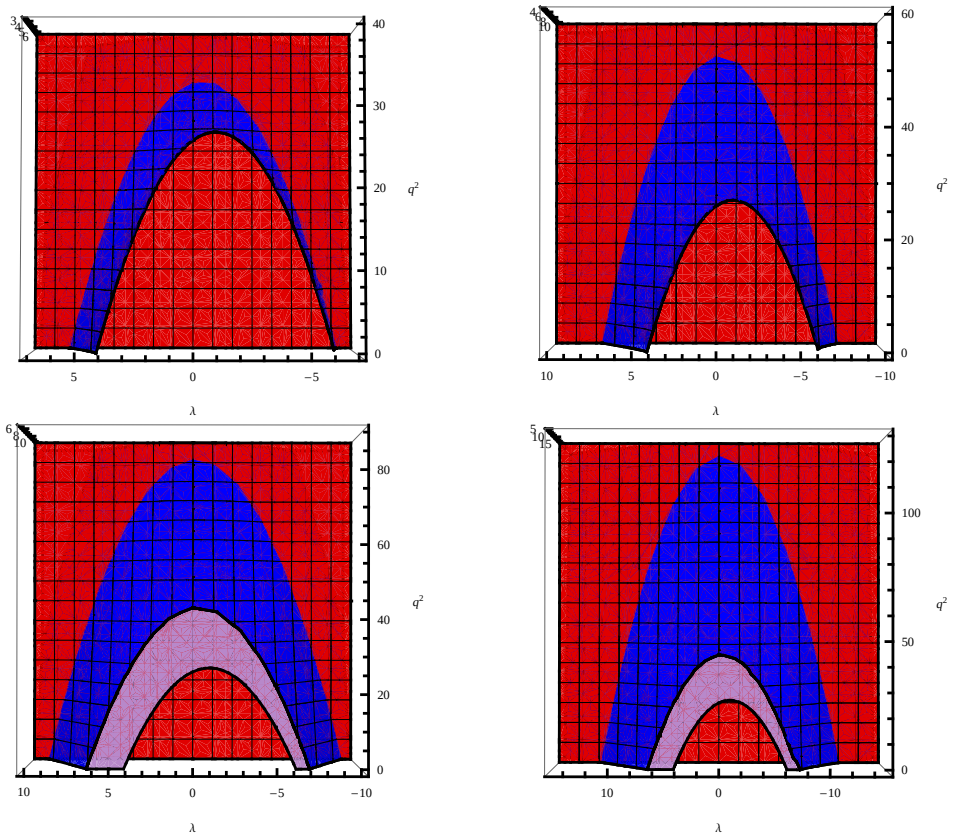

Figure 5.4: The outer red area represents null geodesics that don't reach the observer, whereas the inner red area represents null geodesics with complex turning points and the blue (and violet) area represents possible null geodesics that reach the observer in the radial direction. The specific angular momentum is $a = 0.5$ and it is shown for the cases $r_{\rm e} = r_{\rm ms} (= 4.233)$ (top left), $r_{\rm e} = 6$ (top right), $r_{\rm e} = 8$ (bottom left), $r_{\rm e} = 10$ (bottom right).

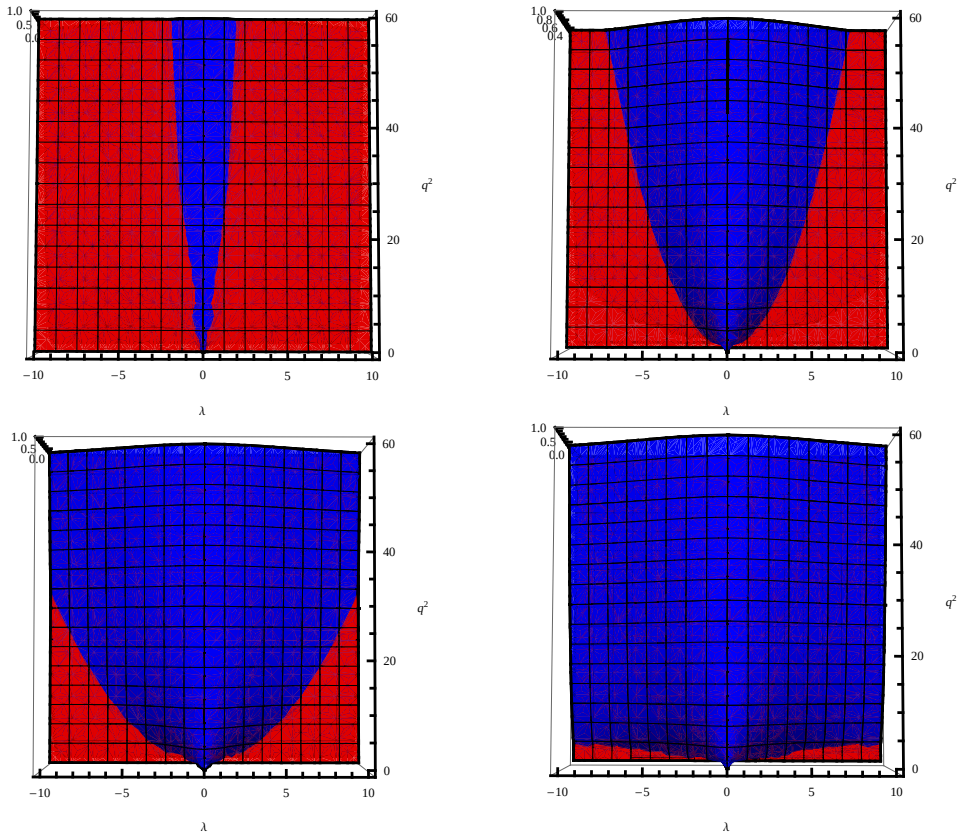

Figure 5.5: The red area represents null geodesics that don't reach the observer, whereas the blue area represents possible null geodesics that reach the observer in the latitudinal direction. The specific angular momentum is $a = 0.5$ and it is for the cases $\theta_e = 15°$ (top left), $\theta_e = 45°$ (top right), $\theta_e = 60°$ (bottom left), $\theta_e = 80°$ (bottom right).

Chapter 6

The r-integral and the θ-integral

The solutions of the Carter equation of the null geodesics (equation 4.19) can be expressed in forms of the elliptic integrals of the first kind, which are defined as

$$F(\varphi, k) = \int_0^{\varphi} \frac{\mathrm{d}\vartheta}{\sqrt{1 - k\sin^2\vartheta}} \tag{6.1}$$

and the complete elliptic integral, which is defined as

$$F\left(\frac{\pi}{2}, k\right) = K(k) = \int_0^{\frac{\pi}{2}} \frac{\mathrm{d}\vartheta}{\sqrt{1 - k\sin^2\vartheta}}. \tag{6.2}$$

The detailed information about the elliptic integrals are in [1], [6].

6.1 The r-integral without a transit through a turning point, real roots

The solution of the r-integral of the null geodesic without turning point r_1 in the radial direction

$$\int_{r_\mathrm{e}}^{\infty} \frac{\mathrm{d}r}{\sqrt{R(r, \lambda, q^2)}} = \int_{r_1}^{\infty} \frac{\mathrm{d}r}{\sqrt{R(r, \lambda, q^2)}} - \int_{r_1}^{r_\mathrm{e}} \frac{\mathrm{d}r}{\sqrt{R(r, \lambda, q^2)}} \tag{6.3}$$

is the elliptic integral of the first kind in the form

$$\int_{r_\mathrm{e}}^{\infty} \frac{\mathrm{d}r}{\sqrt{R(r, \lambda, q^2)}} = g_r[F(\varphi_\mathrm{o}, k_r) - F(\varphi_\mathrm{e}, k_r)], \tag{6.4}$$

where

$$g_r(\lambda, q^2) = \frac{2}{\sqrt{(r_1 - r_3)(r_2 - r_4)}}, \tag{6.5}$$

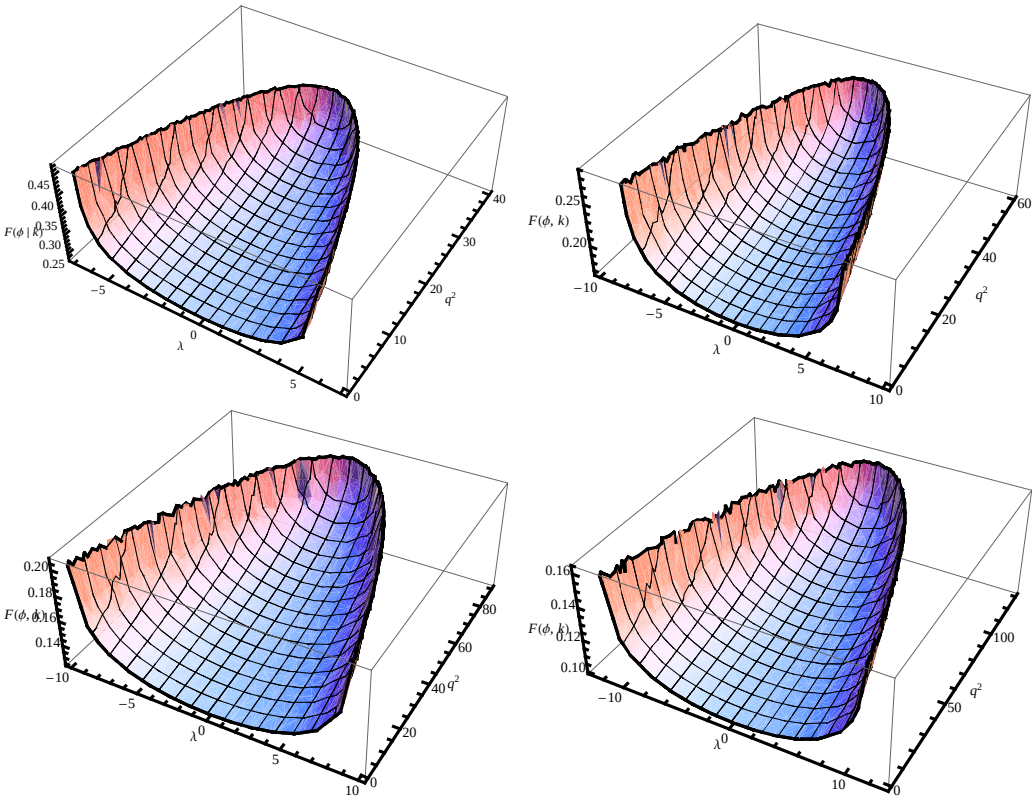

Figure 6.1: The behavior of r-integrals, $r_{\mathrm{e}} = r_{\mathrm{ms}} (= 4.233)$ (top left), $r_{\mathrm{e}} = 6$ (top right), $r_{\mathrm{e}} = 8$ (bottom left), $r_{\mathrm{e}} = 10$ (bottom right). All cases are shown for $a = 0.5$.

$$k_r(\lambda, q^2) = \frac{(r_2 - r_3)(r_1 - r_4)}{(r_1 - r_3)(r_2 - r_4)}, \tag{6.6}$$

$$\varphi_{\mathrm{o}}(\lambda, q^2) = \arcsin\left(\sqrt{\frac{r_2 - r_4}{r_1 - r_4}}\right) \tag{6.7}$$

and

$$\varphi_{\mathrm{e}}(\lambda, q^2) = \arcsin\left[\sqrt{\frac{(r_2 - r_4)(r_{\mathrm{e}} - r_1)}{(r_1 - r_4)(r_{\mathrm{e}} - r_2)}}\right]. \tag{6.8}$$

We can see the behavior of the r-integrals for various emission radii and $a = 0.5$ in the figure 6.1. The area, where the roots are complex (see figures 5.3 or 5.4), can not be expressed by the help of this elliptic integral. We use for this area another form of elliptic integral that is in relevant section. The area of (λ, q^2) that solve the r-integral is larger for greater emission radii. This rule is accepted for the next solution of the r-integral.

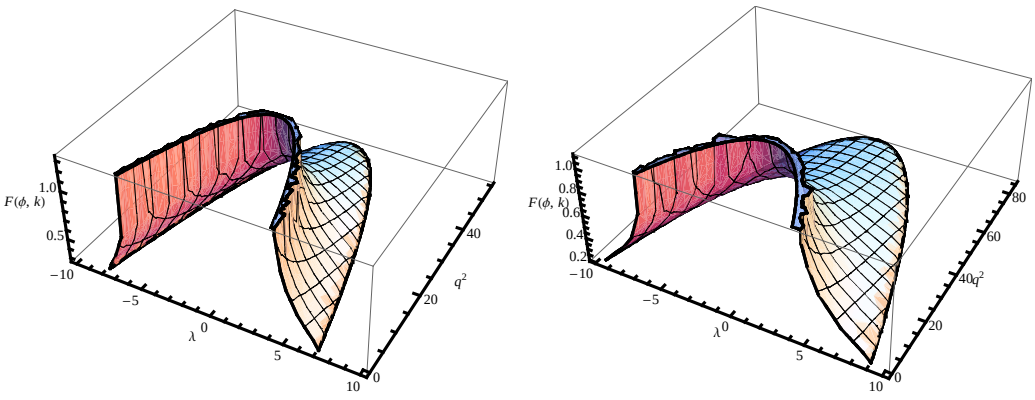

Figure 6.2: The behavior of r-integrals, $r_\mathrm{e} = 6$ (left), $r_\mathrm{e} = 8$ (right). All cases are shown for $a = 0.5$.

6.2 The r-integral with a transit through a turning point, real roots

The solution for this case is analogous as for previous section. We can write the r-integral with the turning point r_1 in the radial direction as

$$\int_{r_\mathrm{e}}^{\infty} \frac{\mathrm{d}r}{\sqrt{R(r,\lambda,q^2)}} = \int_{r_1}^{\infty} \frac{\mathrm{d}r}{\sqrt{R(r,\lambda,q^2)}} + \int_{r_1}^{r_\mathrm{e}} \frac{\mathrm{d}r}{\sqrt{R(r,\lambda,q^2)}} \tag{6.9}$$

and the solution is

$$\int_{r_\mathrm{e}}^{\infty} \frac{\mathrm{d}r}{\sqrt{R(r,\lambda,q^2)}} = g_r[F(\varphi_\mathrm{o}, k_r) + F(\varphi_\mathrm{e}, k_r)], \tag{6.10}$$

where $g_r(\lambda, q^2)$, $k_r(\lambda, q^2)$, $\varphi_\mathrm{o}(\lambda, q^2)$ and $\varphi_\mathrm{e}(\lambda, q^2)$ are the same as in the equations (6.5), (6.6), (6.7) and (6.8). The behavior of the r-integrals for various emission radii and $a = 0.5$ is shown in the figures 6.2.

6.3 The r-integral, $r_1, r_2 \in \mathbb{C}$, $r_3, r_4 \in \mathbb{R}$

If we suppose that two roots are complex ($r_1, r_2 \in \mathbb{C}$) and the other are real ($r_3, r_4 \in \mathbb{R}$) then we can express the complex roots in the form

$$r_1 = u + iv \tag{6.11}$$

and

$$r_2 = u - iv, \tag{6.12}$$

where $u = \frac{1}{2}F$, $v = \frac{1}{2}\sqrt{-\frac{4}{3}A - E - \frac{4B}{F}}$ and A, B, E, F are defined in the equations (4.21), (4.22), (4.25) and (4.21). Now we can write the solution of

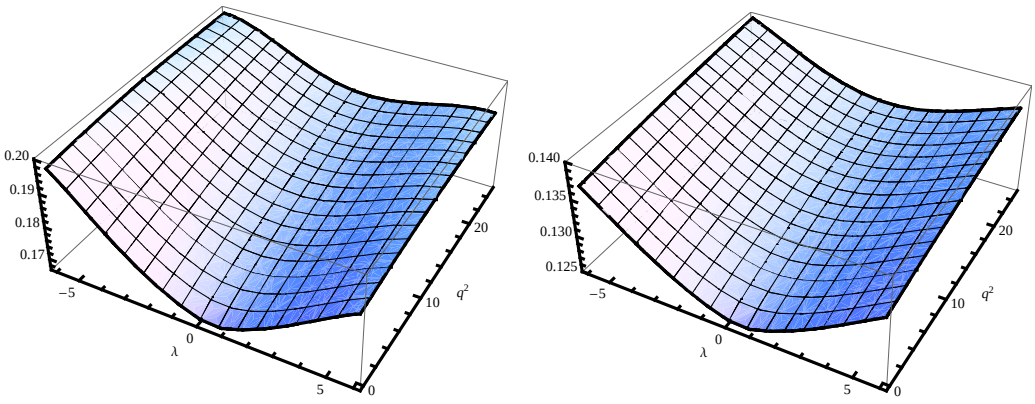

Figure 6.3: The behavior of r-integrals, $r_{\mathrm{e}} = 6$ (left), $r_{\mathrm{e}} = 8$ (right). All cases are shown for $a = 0.5$.

$r-$integral

$$\int_{r_{\mathrm{e}}}^{\infty} \frac{\mathrm{d}r}{\sqrt{R(r,\lambda,q^2)}} = g_r[F(\varphi_{\mathrm{o}}, k_r) - F(\varphi_{\mathrm{e}}, k_r)], \tag{6.13}$$

where

$$g_r(\lambda, q^2) = \frac{1}{\sqrt{AB}}, \tag{6.14}$$

$$k_r(\lambda, q^2) = \frac{(A+B)^2 - (r_3 - r_4)^2}{4AB}, \tag{6.15}$$

$$\varphi_{\mathrm{o}}(\lambda, q^2) = \arccos\left[\frac{A-B}{A+B}\right], \tag{6.16}$$

$$\varphi_{\mathrm{e}}(\lambda, q^2) = \arccos\left[\frac{(A-B)r_{\mathrm{e}} + r_3 B - r_4 A}{(A+B)r_{\mathrm{e}} - r_3 B - r_4 A}\right], \tag{6.17}$$

$$A(\lambda, q^2) = \left[(r_3 - u)^2 + v^2\right]^{1/2} \tag{6.18}$$

and

$$B(\lambda, q^2) = \left[(r_4 - u)^2 + v^2\right]^{1/2}. \tag{6.19}$$

This solution can be used only for area of the pairs (λ, q^2), where the roots r_1, r_2 are complex (the area is shown in the figures 5.3 and 5.4). The behavior of the solution is in the figure 6.3.

6.4 The θ-integral without a transit through a turning point

The solution of the θ-integral without the turning point in the latitudinal direction is the elliptic integral of first kind

$$\int_{0}^{\mu_{\mathrm{e}}} \frac{\mathrm{d}\mu}{\sqrt{\Theta(\mu,\lambda,q^2)}} = \frac{g_\mu}{a} F(\psi, k_\mu), \tag{6.20}$$

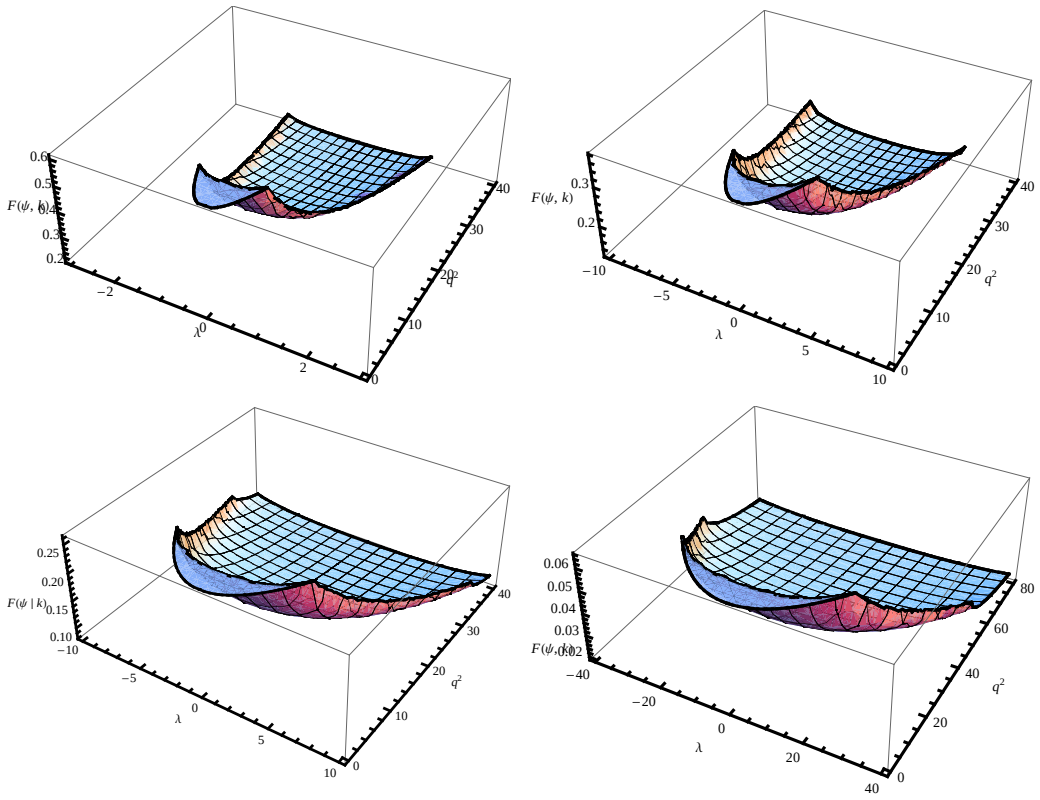

Figure 6.4: The behavior of θ-integrals, $\theta_e = 15°$ (top left), $\theta_e = 45°$ (top right), $\theta_e = 60°$ (bottom left), $\theta_e = 80°$ (bottom right). All cases are shown for $a = 0.5$.

where

$$g_\mu(\lambda, q^2) = \frac{1}{\sqrt{\mu_+^2 + \mu_-^2}}, \tag{6.21}$$

$$k_\mu(\lambda, q^2) = \frac{\mu_+^2}{\mu_+^2 + \mu_-^2}, \tag{6.22}$$

$$\psi(\lambda, q^2) = \arcsin\left[\sqrt{\frac{\mu_o^2(\mu_+^2 + \mu_-^2)}{\mu_+^2(\mu_o^2 + \mu_-^2)}}\right]. \tag{6.23}$$

The behavior of the θ-integrals for various inclinations of observer and $a = 0.5$ is shown in the figures 6.4. The area of all pairs (λ, q^2) that solve θ-integral is larger for greater inclinations of the observer.

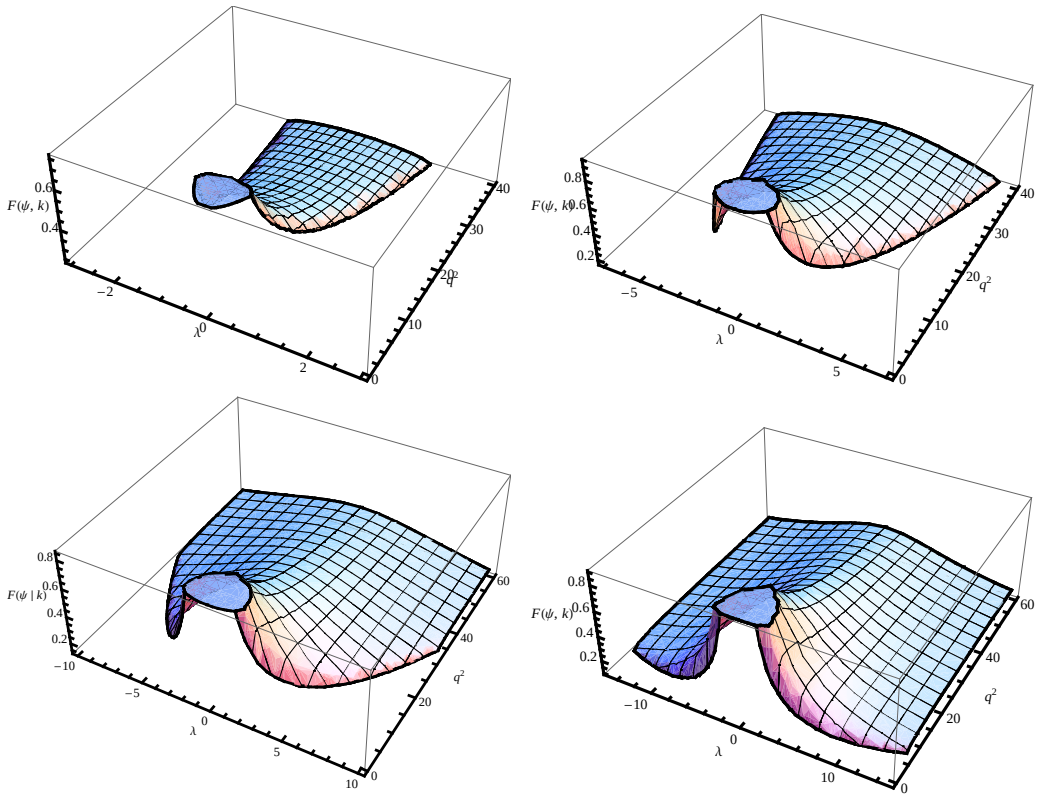

Figure 6.5: The behavior of θ-integrals, $\theta_e = 15°$ (top left), $\theta_e = 45°$ (top right), $\theta_e = 60°$ (bottom left), $\theta_e = 80°$ (bottom right). All cases are shown for $a = 0.5$.

6.5 The θ-integral with one transit through a turning point

If we suppose that the null geodesic in latitudinal direction passes one times trough the turning point μ_+

$$\int_0^{\mu_e} \frac{\mathrm{d}\mu}{\sqrt{\Theta(\mu,\lambda,q^2)}} = 2\int_0^{\mu_+} \frac{\mathrm{d}\mu}{\sqrt{\Theta(\mu,\lambda,q^2)}} - \int_0^{\mu_e} \frac{\mathrm{d}\mu}{\sqrt{\Theta(\mu,\lambda,q^2)}} \tag{6.24}$$

then the solution of θ-integral is

$$\int_0^{\mu_e} \frac{\mathrm{d}\mu}{\sqrt{\Theta(\mu,\lambda,q^2)}} = \frac{g_\mu}{a}[2K(k_\mu) - F(\psi,k_\mu)], \tag{6.25}$$

where g_μ, k_μ and ψ are defined in (6.21), (6.22) and (6.23).

The behavior of the θ-integrals for various inclinations of observer and $a = 0.5$ is shown in the figure 6.5.

Chapter 7

The graphical solution

We can use two techniques to find the minimum and maximum of the function $g(\lambda)$. The first technique is the graphical solution (it will be presented in this chapter) and the second is the technique by the help of the Lagrange multipliers (it will be presented in the following chapter).

We have seen in the previous chapter that there are many solutions for the Carter equation (null geodesics with turning points and without, the turning points can be complex or real, etc.). We must take into account all possible null geodesics (all pairs (λ, q^2) that describe these geodesics) that come to the observer and find between them the minimum and maximum values of λ.

At first we show exemplary solution for $r_{\rm e} = 6$, $a = 0.5$ and $\theta_{\rm e} = 45°$, then we shown how the solution changes for various $r_{\rm e}$, a and $\theta_{\rm e}$.

7.1 An exemplary solution

The Carter equation (4.19) is equality of r-integral and θ-integral. If we plot these integrals in a single two-dimensional graph then the intersection of the two surfaces $R(\lambda, q^2)$ and $\Theta(\lambda, q^2)$ with each other provides the solution of all pairs (λ, q^2) that describe the null geodesics coming to the observer. The null geodesics in this case can be four: i) r-integral without transit trough the turning point and θ-integral without transit trough the turning point, ii) r-integral with transit trough the turning point and θ-integral without transit trough the turning point, iii) r-integral without transit trough the turning point and θ-integral with one transit trough the turning point, iv) r-integral with transit trough the turning point and θ-integral with one transit trough the turning point. Take a look at particular cases.

i) *the r-integral without a transit through the turning point and θ-integral without a transit through the turning point:* The intersection of r-integral and θ-integral is shown in the figure 7.1. We see that the intersection is a curve that comes trough the region where the roots r_1 and r_2 (the turning points) are complex (see figure 5.3 or 5.4). That's why we must use the solution of

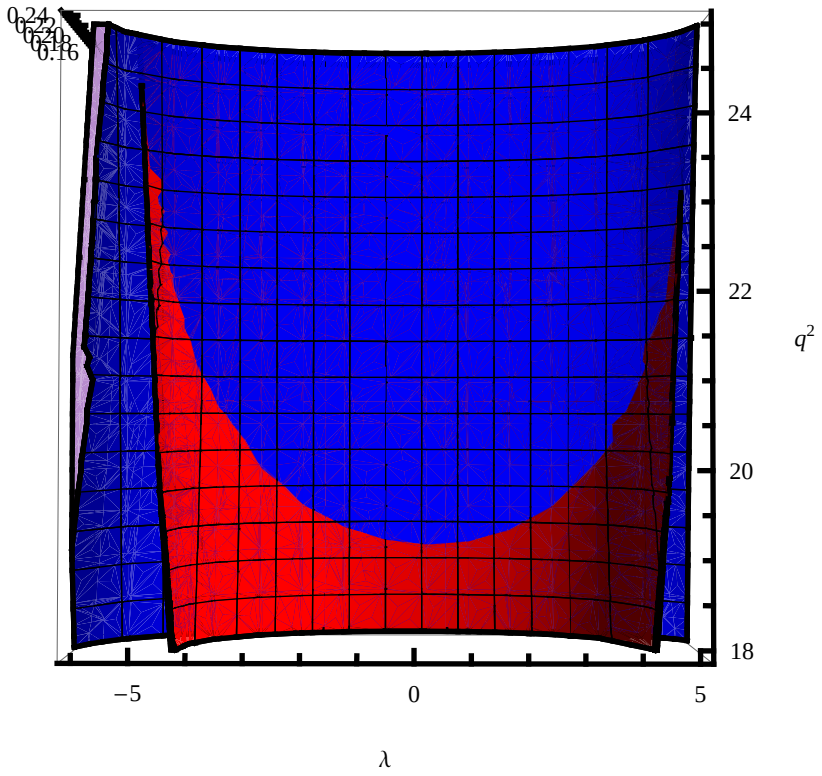

Figure 7.1: The intersection of r-integral (blue) and θ-integral (red). The intersection goes from $\lambda \sim -5$ to $\lambda \sim 5$. The null geodesics does not transit through any turning point, $r_e = 6$, $a = 0.5$ and $\theta_e = 45°$.

r-integral for the complex roots for this region. The solution is shown in the figure 7.2. These both solutions give us the total solution for this case.

ii) *the r-integral with a transit through the turning point and θ-integral without a transit through the turning point:* In this case the intersection does not exist how we could see in the figure 7.3.

iii) *the r-integral without a transit through the turning point and θ-integral with one transit through the turning point:* The solution of this case is again a intersection of the r-integral and θ-integral. We can see it in the figure 7.4. The intersection begins always there where the intersection from the previous case ended. The solution of particular cases tie together.

iv) *the r-integral with a transit through the turning point and θ-integral with one transit through the turning point:* The intersection is shown in the figure 7.5. The curve of the intersection begins again where the previous curve ended and finally the particular intersections create a pent curve of all pairs (λ, q^2) that describe null geodesics that come to the observer. The conclusion that possible pairs (λ, q^2) lie on the pent curve is also in the work of Beckwith and Done [4], but they don't specify what parts of the curve correspond to possible null geodesics.

If we suppose the null geodesics that pass more than one times trough the

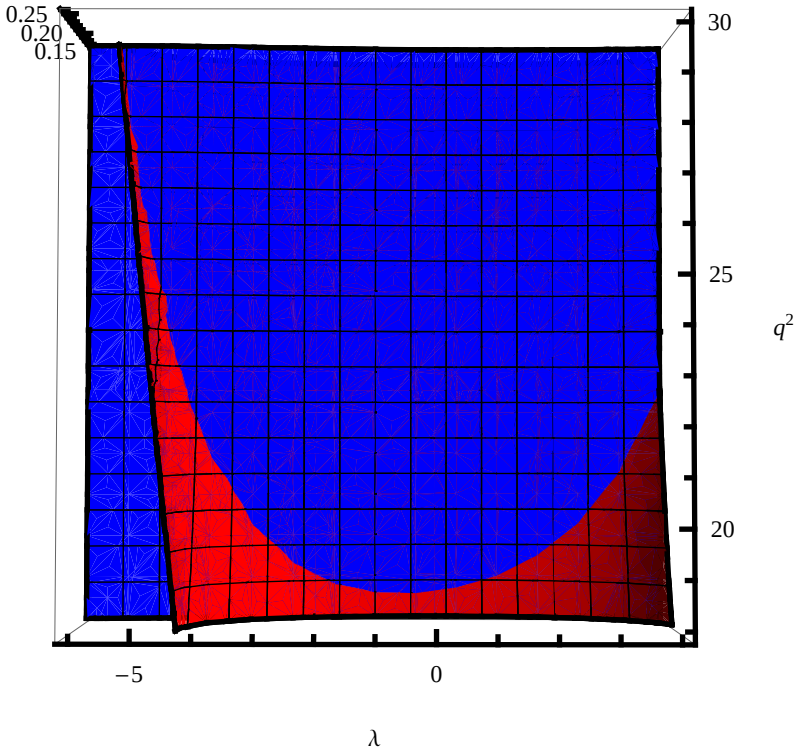

Figure 7.2: The intersection of r-integral (blue) and θ-integral (red) for complex r_1 and r_2. $r_\mathrm{e} = 6$, $a = 0.5$ and $\theta_\mathrm{e} = 45°$.

turning point in the latitudinal direction, we will find out that there in no intersection between the r-integral and θ-integral. There are only three kind of null geodesics that come to the observer at infinity, they are: i) without a transit through the turning point in the radial and latitudinal direction, ii) without a transit through the turning point in the radial direction and with one transit through the turning point in the latitudinal direction, with transit through the turning point in the radial and the latitudinal direction. This is fall-out of the solution.

All these geodesics give us a range of values of λ. If we take a look at the graphs (figures 7.1, 7.2, 7.4, 7.5), we can estimate the minimum and maximum value of λ. It is approximately $\lambda_\mathrm{min} \sim -5$ and $\lambda_\mathrm{max} \sim 5$ and then the values of $g(\lambda)$ are $g_\mathrm{min}(\lambda_\mathrm{min}) \sim 0.55$ and $g_\mathrm{max}(\lambda_\mathrm{max}) \sim 1.1$ (for $r_\mathrm{e} = 6$, $a = 0.5$ and $\theta_\mathrm{o} = 45°$).

7.2 Dependence of the solution on r_e

We can ask how does the solution change if we will assume greater emission radius r_e. The answer is that the curve of possible pairs (λ, q^2) is larger, which means that there are more possible null geodesics that come to the observer and the range of λ is greater. Although the range of λ is greater (and

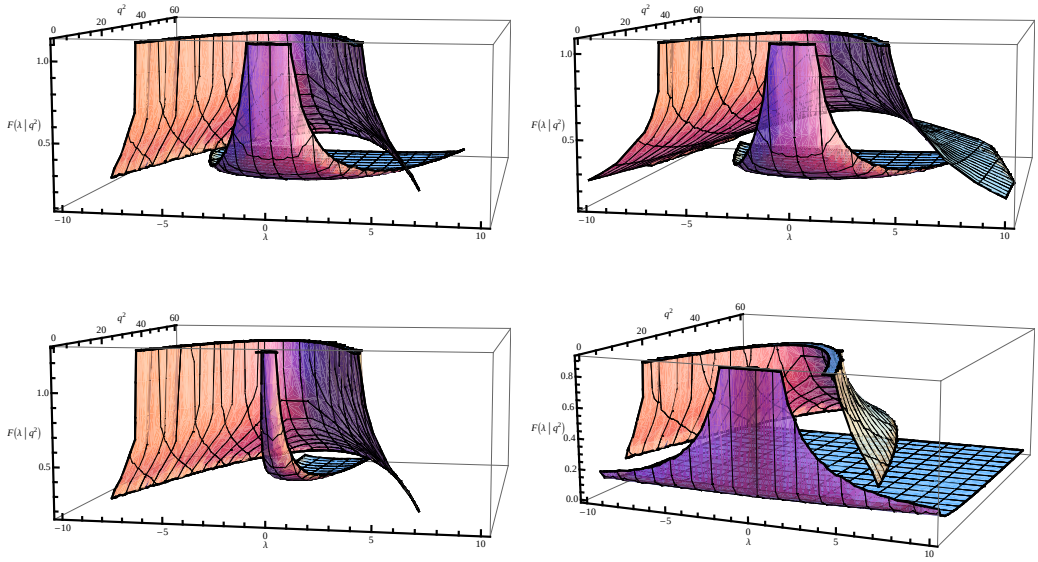

Figure 7.3: The r-integral and θ-integral. There is no intersection if we suppose that the null geodesic transit through the turning point in radial direction and does not in latitudinal direction. The graphs are for $r_{\mathrm{e}} = 6$ and $\theta_{\mathrm{o}} = 45°$ (top left), $r_{\mathrm{e}} = 8$ and $\theta_{\mathrm{o}} = 45°$ (top right), $r_{\mathrm{e}} = 6$ and $\theta_{\mathrm{o}} = 15°$ (bottom left), $r_{\mathrm{e}} = 6$ and $\theta_{\mathrm{o}} = 80°$ (bottom right). The specific angular momentum of black hole is $a = 0.5$ for all cases.

the range of q^2), the change of the emission frequency is smaller, because the effect of the gravitational redshift is smaller for greater r_{e}. The minimum and maximum values are: $g_{\mathrm{min}} \sim 0.55$ and $g_{\mathrm{max}} \sim 1.1$ for $r_{\mathrm{o}} = 6$; $g_{\mathrm{min}} \sim 0.6$ and $g_{\mathrm{max}} \sim 1.1$ for $r_{\mathrm{e}} = 8$; $g_{\mathrm{min}} \sim 0.7$ and $g_{\mathrm{max}} \sim 1.1$ for $r_{\mathrm{e}} = 8$, others parameters are $a = 0.5$, $\theta_{\mathrm{o}} = 45°$.

It is also interesting that the null geodesics with the complex roots r_1 and r_2 do not exist for these larger r_{e}, but exist for small radii (e.g. r_{ms}).

Overall the range of λ increases for greater r_{e}, but the redshift effect is smaller and contrariwise if the emission radius decreases to r_{ms} then range of possible λ is smaller but the effect of the gravitational redshift increases.

7.3 Dependence of the solution on a

The increasing specific angular momentum a of the black hole does not change visibly the range of λ, how we can see in the figure 7.6, we suppose fixed r_{e}. But it does not mean that the minimum and maximum of $g(\lambda)$ do not change. The parameters a and r_{e} change the behavior of the function $g(\lambda)$, how it is shown in figures 5.1 and 5.2. The range of λ is same, but the behavior of $g(\lambda)$ differentiates and in the end we other minimum and

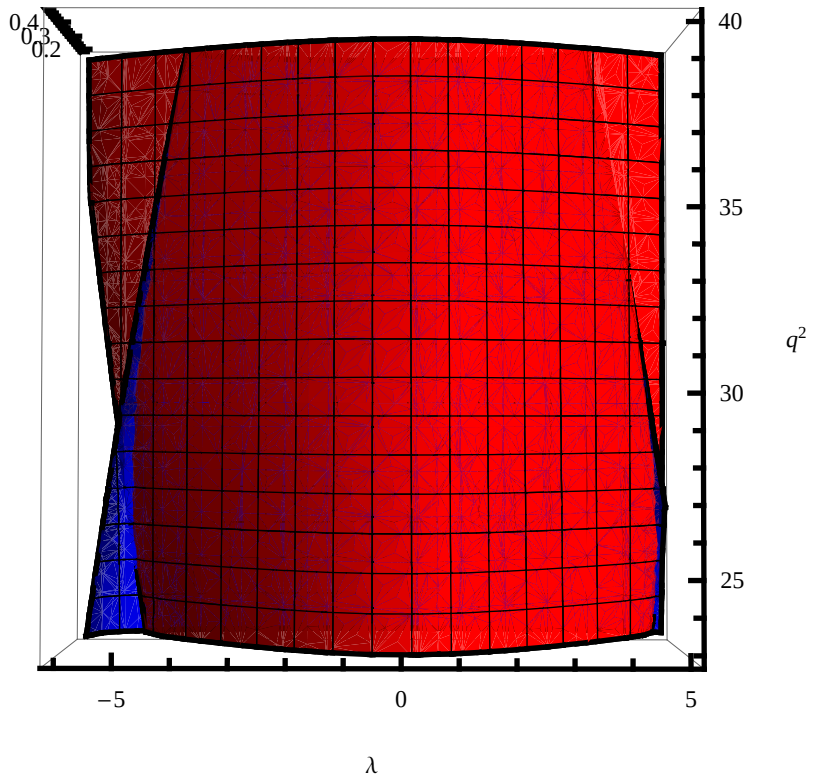

Figure 7.4: The intersection of r-integral (blue) and θ-integral (red). The intersection has two parts, one goes from $q^2 \sim 25$ to $q^2 \sim 40$ and second goes from $q^2 \sim 23$ to $q^2 \sim 34$ The null geodesics transit through the turning point in latitudinal direction, $r_e = 6$, $a = 0.5$ and $\theta_e = 45°$.

maximum of $g(\lambda)$.

Special case is when we have emission radius $r_e = r_{ms}$. If we change the specific angular momentum a then the r_{ms} must change too, because r_{ms} depends on a (equation (4.11)). How we have seen in previous section, the range of λ changes with emission radius, then for this case the range of λ changes with a. If a increases then r_{ms} decreases and the range of λ is smaller. We can remark in figure 5.2 that $g(\lambda)$ takes the values smaller than 1 for extreme a with emission on r_{ms}. The effect of gravitational redshift is greater than for larger r_e.

7.4 Dependence of the solution on θ_o

If the observer has a small inclination (e.g. $\theta_o = 15°$) then we should observe mainly the gravitational redshift. If we suppose great inclinations, we should observe redshift and blueshift. The graphical solution gives us the minimum value $\lambda_{min} \sim -2$ and the maximum value $\lambda_{max} \sim 2$ that correspond to: $g_{min} \sim 0.74$ and $g_{max} \sim 0.88$ for the inclination $\theta_o = 15°$ ($r_e = 8$, $a = 0.5$). Assume $\theta_o = 15°$, $r_e = 8$, $a = 0.5$ then the minimum of $g(\lambda)$ is $g_{min} \sim 0.5$

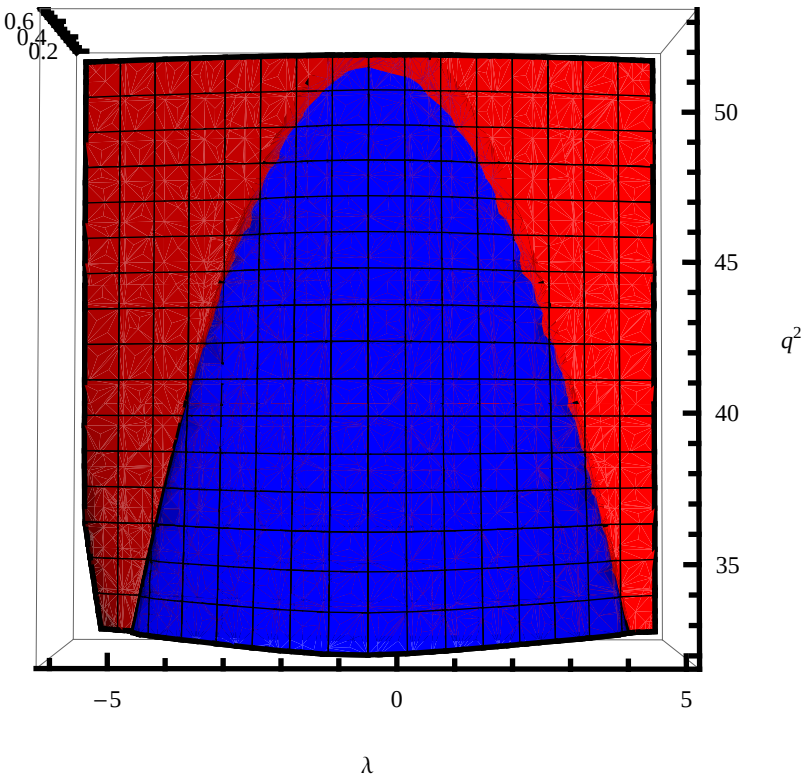

Figure 7.5: The intersection of r-integral (blue) and θ-integral (red). The null geodesics transit through turning point in the radial and latitudinal direction, $r_{\rm e} = 6$, $a = 0.5$ and $\theta_{\rm e} = 45°$.

and the maximum of $g(\lambda)$ is $g_{\rm max} \sim 1.35$.

Another result is that for small inclination there are only two kinds of null geodesics: without the turning point in radial and latitudinal direction, without turning point in radial direction and with one transit in latitudinal direction. If the inclination increase then appears third kind of the null geodesic: with turning point in radial and latitudinal direction.

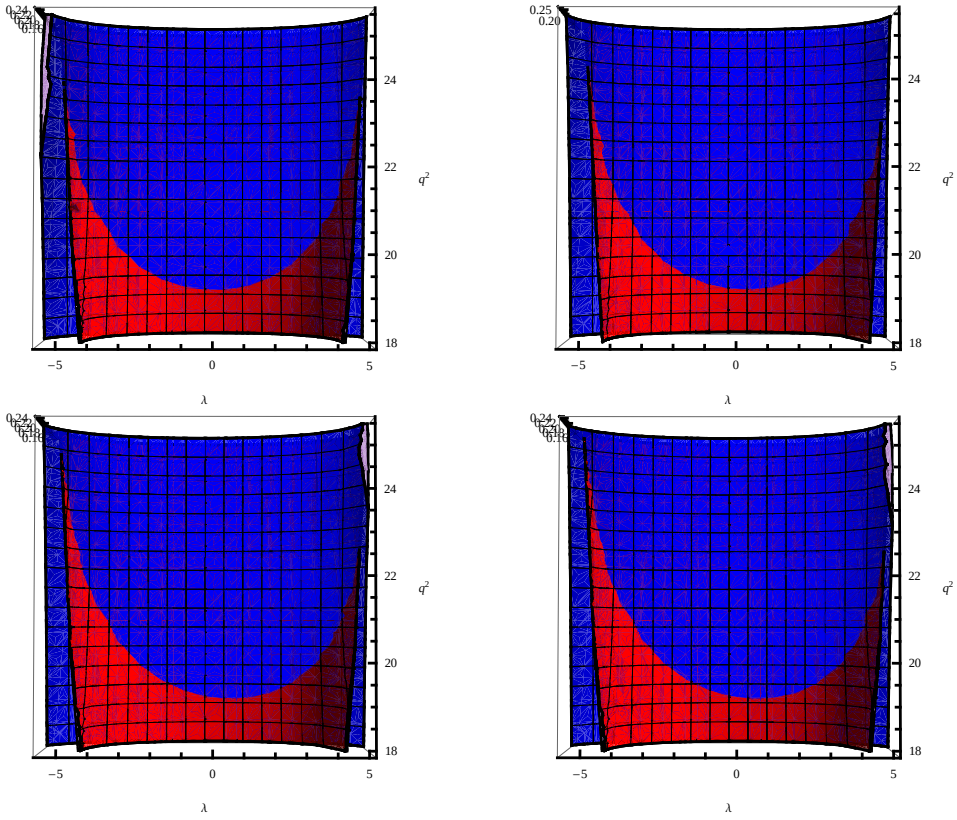

Figure 7.6: The intersection between r-integral (without the transit through the turning point) and θ-integral (without the transit through the turning point), $r_{\mathrm{e}} = 6$, $\theta_{\mathrm{o}} = 45°$. The graphs are for the cases $a = 0.1$, $a = 0.5$, $a = 0.9$ and $a = 0.998$.

Chapter 8

The solution by the help of the Lagrange multipliers

8.1 Lagrange multipliers

We will present in this chapter how to find the minimum and the maximum of the function (5.4) by the help of the analytic procedure. The procedure that we use is called Lagrange multipliers.

Lagrange multipliers are used to find the extremes of the function $f(x_1, .., x_n)$ where the variables $(x_1, .., x_n)$ corresponding to extremes must fulfil the constraint $g(x_1, .., x_n) = 0$. We will suppose for the simplicity that the function $f(x_1, .., x_n)$ is $f(x, y)$ and the constraint $g(x_1, .., x_n) = g(x, y) = 0$. Now define the Lagrangian as

$$\Lambda(x, y, \lambda) = f(x, y) - \lambda g(x, y), \tag{8.1}$$

where λ is the Lagrange multiplier. The partial derivatives of the Lagrangian must satisfy

$$\frac{\partial}{\partial x}\Lambda(x, y, \lambda) = 0, \tag{8.2}$$

$$\frac{\partial}{\partial y}\Lambda(x, y, \lambda) = 0, \tag{8.3}$$

$$\frac{\partial}{\partial \lambda}\Lambda(x, y, \lambda) = 0. \tag{8.4}$$

These are three equation for three unknown. If we solve them then we found the x and y that correspond to the extremes of the function $f(x, y)$ with a constraint $g(x, y) = 0$.

8.2 The analytic procedure to find extremes of ratio $g(\lambda)$

We looking for extremes of the function (5.4) with the constraint Carter equation (4.19). Then the Lagrangian Λ is in the form (the Lagrange multi-

plier λ is termed as α here)

$$\Lambda(\lambda, q^2, \alpha) = \frac{1}{u^t}\frac{1}{1-\lambda\Omega} - \alpha \int\limits_{r_\mathrm{e}}^{\infty} \frac{\mathrm{d}r}{\sqrt{R(r,\lambda,q^2)}} + \alpha \int\limits_{0}^{\mu_\mathrm{o}} \frac{\mathrm{d}\mu}{\sqrt{\Theta(\mu,\lambda,q^2)}}. \qquad (8.5)$$

Before we write the partial derivatives of the Lagrangian (8.5) we have to tell which null geodesic we solve. We know that there are tree kind of null geodesics (from the graphical solution) and now we write their Lagrangian and its partial derivative.

i) *The null geodesics without a transit through the turning points:* The lagrangian is in the form

$$\begin{aligned}\Lambda(\lambda, q^2, \alpha) &= \frac{1}{u^t}\frac{1}{1-\lambda\Omega} - \alpha \int\limits_{r_1}^{\infty} \frac{\mathrm{d}r}{\sqrt{R(r,\lambda,q^2)}} \\ &\quad + \alpha \int\limits_{r_1}^{r_\mathrm{e}} \frac{\mathrm{d}r}{\sqrt{R(r,\lambda,q^2)}} + \alpha \int\limits_{0}^{\mu_\mathrm{o}} \frac{\mathrm{d}\mu}{\sqrt{\Theta(\mu,\lambda,q^2)}} \qquad (8.6)\end{aligned}$$

or in the form of the elliptic integrals of first kind that solve the r-integral and θ-integral

$$\Lambda(\lambda, q^2, \alpha) = \frac{1}{u^t}\frac{1}{1-\lambda\Omega} - \alpha g_r F(\varphi_\mathrm{o}, k_r) + \alpha g_r F(\varphi_\mathrm{e}, k_r) + \alpha \frac{g_\mu}{a} F(\psi, k_\mu), \quad (8.7)$$

where $g_r F(\varphi_\mathrm{o}, k_r)$ and $g_r F(\varphi_\mathrm{e}, k_r)$ are defined in (6.4) for real roots and in (6.13) for complex roots, $\frac{g_\mu}{a} F(\psi, k_\mu)$ is defined in (6.20).

The partial derivatives of the Lagrangian (8.7) are

$$\begin{aligned}\frac{\partial}{\partial\lambda}\Lambda(\lambda, q^2, \alpha) &= \frac{1}{u^t}\frac{\Omega}{(1-\lambda\Omega)^2} - \alpha\frac{\partial}{\partial\lambda}[g_r F(\varphi_\mathrm{o}, k_r)] \\ &\quad + \alpha\frac{\partial}{\partial\lambda}[g_r F(\varphi_\mathrm{e}, k_r)] + \alpha\frac{\partial}{\partial\lambda}[\frac{g_\mu}{a} F(\psi, k_\mu)] = 0, \quad (8.8)\end{aligned}$$

$$\begin{aligned}&\frac{\partial}{\partial q^2}\Lambda(\lambda, q^2, \alpha) = \\ &\qquad \alpha\left\{\frac{\partial}{\partial q^2}[g_r F(\varphi_\mathrm{o}, k_r) - g_r F(\varphi_\mathrm{e}, k_r) - \frac{g_\mu}{a} F(\psi, k_\mu)]\right\} = 0, \qquad (8.9)\end{aligned}$$

$$\frac{\partial}{\partial\alpha}\Lambda(\lambda, q^2, \alpha) = g_r F(\varphi_\mathrm{o}, k_r) - g_r F(\varphi_\mathrm{e}, k_r) - \frac{g_\mu}{a} F(\psi, k_\mu) = 0. \qquad (8.10)$$

We see from the equation (8.9) that $\alpha = 0$ or $\frac{\partial}{\partial q^2}[g_r F(\varphi_\mathrm{o}, k_r) - g_r F(\varphi_\mathrm{e}, k_r) - \frac{g_\mu}{a} F(\psi, k_\mu)] = 0$. The Lagrange multiplier can not be zero, because the equation (8.8) has no solution for $\alpha = 0$ and that's why we suppose

$$\frac{\partial}{\partial q^2}[g_r F(\varphi_\mathrm{o}, k_r) - g_r F(\varphi_\mathrm{e}, k_r) - \frac{g_\mu}{a} F(\psi, k_\mu)] = 0. \qquad (8.11)$$

Now we have two equation (8.10) and (8.11) for two unknown λ and q^2. If we find these (λ, q^2) then we found the values of λ that correspond to the values of minimum and maximum of $g(\lambda)$.

ii) *The null geodesics with one transit through a turning point in latitudinal direction:* In this case the Lagrangian (8.5) is

$$\begin{aligned}\Lambda(\lambda, q^2, \alpha) &= \frac{1}{u^t}\frac{1}{1-\lambda\Omega} - \alpha g_r F(\varphi_{\rm o}, k_r) + \alpha g_r F(\varphi_{\rm e}, k_r) \\ &\quad + \alpha\frac{2g_\mu}{a}K(k_\mu) - \alpha\frac{g_\mu}{a}F(\psi, k_\mu). \end{aligned} \tag{8.12}$$

If we use the procedure from the previous case, we obtain two equations

$$g_r F(\varphi_{\rm o}, k_r) - g_r F(\varphi_{\rm e}, k_r) - \frac{2g_\mu}{a}K(k_\mu) + \frac{g_\mu}{a}F(\psi, k_\mu) = 0 \tag{8.13}$$

and

$$\frac{\partial}{\partial q^2}[g_r F(\varphi_{\rm o}, k_r) - g_r F(\varphi_{\rm e}, k_r) - \frac{2g_\mu}{a}K(k_\mu) + \frac{g_\mu}{a}F(\psi, k_\mu)] = 0. \tag{8.14}$$

iii) *The null geodesics with transits through the turning points in radial and latitudinal direction:* The Lagrangian (8.5) is

$$\begin{aligned}\Lambda(\lambda, q^2, \alpha) &= \frac{1}{u^t}\frac{1}{1-\lambda\Omega} - \alpha g_r F(\varphi_{\rm o}, k_r) - \alpha g_r F(\varphi_{\rm e}, k_r) \\ &\quad + \alpha\frac{2g_\mu}{a}K(k_\mu) - \alpha\frac{g_\mu}{a}F(\psi, k_\mu). \end{aligned} \tag{8.15}$$

The resulting two equations are

$$g_r F(\varphi_{\rm o}, k_r) + g_r F(\varphi_{\rm e}, k_r) - \frac{2g_\mu}{a}K(k_\mu) + \frac{g_\mu}{a}F(\psi, k_\mu) = 0 \tag{8.16}$$

and

$$\frac{\partial}{\partial q^2}[g_r F(\varphi_{\rm o}, k_r) + g_r F(\varphi_{\rm e}, k_r) - \frac{2g_\mu}{a}K(k_\mu) + \frac{g_\mu}{a}F(\psi, k_\mu)] = 0. \tag{8.17}$$

Now we have all formulas to find out the extremes of the function $g(\lambda)$ (5.4).

8.3 The derivatives of the elliptic integrals of the first kind

We need know the derivatives of the elliptic integrals to solve the equations (8.10) and (8.11), (8.13) and (8.14), (8.16) and (8.17), but at first we define some auxiliary terms

$$r_1' = \frac{\partial r_1}{\partial q^2}, r_2' = \frac{\partial r_2}{\partial q^2}, r_3' = \frac{\partial r_3}{\partial q^2}, r_4' = \frac{\partial r_4}{\partial q^2}, \mu_-' = \frac{\partial \mu_-}{\partial q^2}, \mu_+' = \frac{\partial \mu_+}{\partial q^2}, \tag{8.18}$$

where r_1, r_2, r_3, r_4, μ_+ and μ_- are defined in (4.28), (4.29), (4.30), (4.31), (4.32) and (4.33).

i) The derivative of $g_r F(\varphi_\mathrm{e}, k_r)$ (6.4), (6.10) is for $r_1, r_2, r_3, r_4 \in \mathbb{R}$

$$\frac{\partial}{\partial q^2}[g_r F(\varphi_\mathrm{e}, k_r)] = -GF(\varphi_\mathrm{e}, k_r) + g_r \left[H + I \left(J - \frac{F(\varphi_\mathrm{e}, k_r)}{2(k_r - 1)} \right) \right], \quad (8.19)$$

where

$$G = \frac{(r_2 - r_4)(r_1' - r_3') + (r_1 - r_3)(r_2' - r_4')}{[(r_1 - r_3)(r_2 - r_4)]^{3/2}}, \quad (8.20)$$

$$H = \frac{-\frac{(r_1' - r_4')}{(r_1 - r_4)} + \frac{(r_2' - r_4')}{(r_2 - r_4)} - \frac{r_1'}{(r_e - r_1)} + \frac{r_2'}{(r_e - r_2)}}{2\sqrt{\beta}\sqrt{1-\beta}\sqrt{1 - \frac{(r_2 - r_3)(r_e - r_1)}{(r_1 - r_3)(r_e - r_2)}}} \beta, \quad (8.21)$$

$$I = \left[-\frac{r_1' - r_3'}{r_1 - r_3} + \frac{r_2' - r_3'}{r_2 - r_3} + \frac{r_1' - r_4'}{r_1 - r_4} - \frac{r_2' - r_4'}{r_2 - r_4} \right] k_r, \quad (8.22)$$

$$J = \frac{\sin[2 \arcsin \sqrt{\beta}]}{4(k_r - 1)\sqrt{1 - \frac{(r_2 - r_3)(r_e - r_1)}{(r_1 - r_3)(r_e - r_2)}}}, \quad (8.23)$$

and

$$\beta = \frac{(r_2 - r_4)(r_e - r_1)}{(r_1 - r_4)(r_e - r_2)}. \quad (8.24)$$

ii) The derivative of $g_r F(\varphi_\mathrm{o}, k_r)$ (6.4), (6.10) is for $r_1, r_2, r_3, r_4 \in \mathbb{R}$

$$\frac{\partial}{\partial q^2}[g_r F(\varphi_\mathrm{o}, k_r)] = -GF(\varphi_\mathrm{o}, k_r) + g_r \left[H + I \left(J - \frac{F(\varphi_\mathrm{o}, k_r)}{2(k_r - 1)} \right) \right], \quad (8.25)$$

where

$$G = \frac{(r_2 - r_4)(r_1' - r_3') + (r_1 - r_3)(r_2' - r_4')}{[(r_1 - r_3)(r_2 - r_4)]^{3/2}}, \quad (8.26)$$

$$H = \frac{-\frac{(r_1' - r_4')}{(r_1 - r_4)} + \frac{(r_2' - r_4')}{(r_2 - r_4)}}{2\sqrt{\gamma}\sqrt{1-\gamma}\sqrt{1 - \frac{r_2 - r_3}{r_1 - r_3}}} \gamma, \quad (8.27)$$

$$I = \left[-\frac{r_1' - r_3'}{r_1 - r_3} + \frac{r_2' - r_3'}{r_2 - r_3} + \frac{r_1' - r_4'}{r_1 - r_4} - \frac{r_2' - r_4'}{r_2 - r_4} \right] k_r, \quad (8.28)$$

$$J = \frac{\sin[2 \arcsin \sqrt{\gamma}]}{4(k_r - 1)\sqrt{1 - \frac{r_2 - r_3}{r_1 - r_3}}}, \quad (8.29)$$

and

$$\gamma = \frac{r_2 - r_4}{r_1 - r_4}. \quad (8.30)$$

iii) The derivative of $g_r F(\varphi_\mathrm{e}, k_r)$ (6.13) is for $r_1, r_2 \in \mathbb{C}$, $r_3, r_4 \in \mathbb{R}$

$$g_r F(\varphi_\mathrm{e}, k_r) = -\frac{BA' + AB'}{2(AB)^{3/2}} F(\varphi_\mathrm{e}, k_r) + (-G + HI), \quad (8.31)$$

where

$$G = \frac{(\sigma+1)(r_1B' + r_1'B + r_eB') + (\sigma-1)(r_2A' + r_2'A - r_eA')}{[(A+B)r_e - Br_3 - Ar_4]\sqrt{1-\sigma^2}\sqrt{1-k_r(1-\sigma^2)}}, \tag{8.32}$$

$$H = -(\frac{A'}{A} + \frac{B'}{B})k_r + \frac{2(A+B)(A'+B') - 2(r_3-r_4)(r_3'-r_4')}{4AB}, \tag{8.33}$$

$$I = \frac{F(\varphi_e, k_r)}{2(1-k_r)} + \frac{\sin[2\arccos\sigma]}{4(k_r-1)\sqrt{1-k_r(1-\sigma^2)}}, \tag{8.34}$$

$$\sigma = \frac{(A-B)r_e + Br_1 - Ar_2}{(A+B)r_e - Br_1 - Ar_2}, \tag{8.35}$$

$$A' = \frac{2(r_1-u)(r_1'-u') + 2vv'}{2\sqrt{(r_1)^2+v^2}}, \tag{8.36}$$

$$B' = \frac{2(r_2-u)(r_2'-u') + 2vv'}{2\sqrt{(r_2)^2+v^2}}. \tag{8.37}$$

iv) The derivative of $g_rF(\varphi_o, k_r)$ (6.13) is for $r_1, r_2 \in \mathbb{C}$, $r_3, r_4 \in \mathbb{R}$

$$g_rF(\varphi_o, k_r) = -\frac{BA' + AB'}{2(AB)^{3/2}}F(\varphi_o, k_r) + (-G + HI), \tag{8.38}$$

where

$$G = \frac{A' - B' - \omega(A'+B')}{(A+B)\sqrt{1-\omega^2}\sqrt{1-k_r(1-\omega^2)}}, \tag{8.39}$$

$$H = -(\frac{A'}{A} + \frac{B'}{B})k_r + \frac{2(A+B)(A'+B') - 2(r_3-r_4)(r_3'-r_4')}{4AB}, \tag{8.40}$$

$$I = \frac{F(\varphi_e, k_r)}{2(1-k_r)} + \frac{\sin[2\arccos\omega]}{4(k_r-1)\sqrt{1-k_r(1-\omega^2)}}, \tag{8.41}$$

$$\omega = \frac{(A-B)}{(A+B)}, \tag{8.42}$$

$$A' = \frac{2(r_1-u)(r_1'-u') + 2vv'}{2\sqrt{(r_1)^2+v^2}}, \tag{8.43}$$

$$B' = \frac{2(r_2-u)(r_2'-u') + 2vv'}{2\sqrt{(r_2)^2+v^2}}. \tag{8.44}$$

v) The derivative of $g_\mu F(\psi, k_\mu)$ (6.20), (6.24) is

$$\frac{\partial}{\partial q^2}[g_\mu F(\psi, k_\mu)] = GF(\psi, k_\mu) + g_\mu\left[H + I\left(J - \frac{F(\psi, k_\mu)}{2(k_\mu - 1)}\right)\right], \tag{8.45}$$

where

$$G = \frac{\mu_-\mu_-' + \mu_+\mu_+'}{(\mu_+^2 + \mu_+^2)^{3/2}}, \tag{8.46}$$

$$H = \frac{-\mu'_- - \mu'_+ + \frac{\mu'_+ + \mu'_-}{\mu_+ + \mu_-}}{\sqrt{\delta}\sqrt{1-\delta}\sqrt{1 - \frac{\mu_o^2}{\mu_-^2 + \mu_o^2}}}\delta, \tag{8.47}$$

$$I = 2\left[\frac{\mu'_+}{\mu_+} - \frac{\mu_-\mu'_- + \mu_+\mu'_+}{\mu_+^2 + \mu_-^2}\right] k_\mu, \tag{8.48}$$

$$J = \frac{\sin[2\arcsin\sqrt{\delta}]}{4(k_\mu - 1)\sqrt{1 - \frac{\mu_o^2}{\mu_-^2 + \mu_o^2}}}, \tag{8.49}$$

and

$$\delta = \frac{\mu_o^2(\mu_-^2 + \mu_+^2)}{\mu_+^2(\mu_-^2 + \mu_o^2)}. \tag{8.50}$$

vi) The derivative of $g_\mu K(k_\mu)$ (6.24) is

$$\frac{\partial}{\partial q^2}[g_\mu K(k_\mu)] = -GK(k_\mu) + \frac{\sqrt{\mu_-^2 + \mu_+^2}}{\mu_+^2(1-k_\mu)}\frac{I}{2}J, \tag{8.51}$$

where

$$G = \frac{\mu_-\mu'_- + \mu_+\mu'_+}{(\mu_+^2 + \mu_+^2)^{3/2}}, \tag{8.52}$$

$$I = 2\left[\frac{\mu'_+}{\mu_+} - \frac{\mu_-\mu'_- + \mu_+\mu'_+}{\mu_+^2 + \mu_-^2}\right] k_\mu, \tag{8.53}$$

$$J = E(k_\mu) - (1-k_\mu)K(k_\mu). \tag{8.54}$$

$E(k_\mu)$ is the complete elliptic integral of second kind that is defined as

$$E(k) = \int_0^{\frac{\pi}{2}} \sqrt{1 - k\sin^2\theta}\mathrm{d}\theta. \tag{8.55}$$

Chapter 9

Conclusion

Our main goal was to find the procedure (or an analytic formula) to determine the extremes of the function $g(\lambda)$ (5.4). The procedure was found with the help of Lagrange multipliers. We obtained two equations (see the previous chapter) whose solution provides searched extremes. Why do we have two equations to calculate the extremes rather than a single formula that we desired? The answer is evident, because the Carter equation (4.19) depends on two parameters (λ, q^2) (if we know other parameters r_{e}, θ_{o} and a) and from this reason we have two equations for two unknowns. Unfortunately these equations are so much complicated that can be solved only numerically. It is a work for the future to create a program that will be able to solve these equations.

The graphical solution is another way to find the extremes. The graphical solution does not give accurate values but approximate. It does not matter, because we can use this information to optimize the numerical code. More important is that the graphical solution shows what null geodesics come to the observer, and we found out that there are only three possibilities: without a transit through the turning points, with a transit through the turning point in latitudinal direction, and with a transit through the turning point in both the radial and latitudinal directions. The number of types of null geodesics depends on the inclination angle of the observer. For very small inclinations there are only two null geodesics: without a transit through the turning points, with a transit through the turning point in latitudinal direction, and for larger inclinations there are already three kinds.

The dependence on an angular momentum of black hole, an emission radius and an inclination angle of the observer is shown in the chapter 7 Graphical solution. We can see that the shift of the frequency very change and that the wave length depends both on the parameters of system and on the position of observer.

Bibliography

[1] Abramowitz M., Stegun I. A. (1965): *Handbook of Mathematical Functions* Dover, New York.

[2] Abramowicz M. A., Czerny B., Lasota J. P., Szuszkiewicz E. (1988): *Slim accretion disks*, ApJ **332** 646-658.

[3] Balbus S. A., Hawley J. F. (1998): *Instability, turbulence, and enhanced transport in accretion disks*, Reviews of Modern Physics **70** 1-53.

[4] Beckwith K., Done Ch. (2005): *Extreme gravitational lensing near rotating black holes*, Mon. Not. R. Astron. Soc. **359** 1217-1228.

[5] Bradt W. M., McClinctock J. E. (1983): *The optical counterparts of compact galactic X-ray sources*, Ann. Rev. Astron. Astrophys. **21** 13-66.

[6] Byrd P. F., Friedman M. D. (1971): *Handbook of Elliptic Integrals for Engineers and Scientiests*, Springer-Verlag, New York.

[7] Camenzind M. (2007): *Compact objects in Astrophysics*, Springer, Berlin.

[8] Carter B. (1968): *Global Structure of the Kerr Family of Gravitational Fields*, Phys. Rev. **174** 1559.

[9] Chandrasekhar S. (2004): *The Mathematical Theory of Black Holes*, Oxford University Press, Oxford.

[10] Charles P. A., Seward F. D. (1995): *Exploring the X-ray Universe*, Cambridge University Press, Cambridge.

[11] Conti P. S. (1978): *Stellar parameters of five early type companions of X-ray sources*, A&A **63** 225-235.

[12] Davidson K., Ostriker J. P. (1973): *Neutron-Star Accretion in a Stellar Wind: Model for a Pulsed X-Ray Source*, ApJ **179** 585-598.

[13] Frank J., King A., Raine D. (2002): *Accretion Power in Astrophysics*, Cambridge University Press, Cambridge.

[14] Giacconi R., Gursky H., Paolini F. R., Rossi B. B. (1962): *Evidence for X-Ray from Sources outside the Solar System*, Phys. Rev. Lett. **9** 439.

[15] Giacconi R., Gursky H. (1974): *X-Ray Astronomy*, D. Reidel Publ. Co., Dordrecht.

[16] Giacconi R., Ruffini R. (1978): *Physics and Astrophysics of Neutron Stars and Black Holes* North Holland, Amsterdam.

[17] Giacconi R. (1980): *The Einstein X-ray Observatory*, Scientific American **242** 80-85.

[18] Gursky H., Ruffini R. (1975): *Neutron Stars, Black Holes and Binary X-Ray Sources*, Reidel, Dordrecht.

[19] Karas V. (2006): *Theoretical aspects of relativistic spectral features*, Astronomische Nachrichten **327** 961-968.

[20] Kellogg E. M. (1975): *X-ray astronomy in the UHURU epoch and beyond*, Apj **197** 689-691, 693-695, 697-704.

[21] Kerr R. P. (1963): *Gravitational Field of a Spinning Mass as an Example of Algebraically Special Metric*, Phys. Rev. Lett. **11** 237.

[22] Matt G., Perola G. C. (1992): *The iron K-alpha response in an X-ray illuminated relativistic disc and a black hole mass estimate*, MNRAS **259** 433-436.

[23] Narayan R., Yi I. (1994): *Advection-dominated accretion: A self-similar solution*, ApJ **428** L13-L16.

[24] Osterbrock D. E., Ferland G. J. (2006): *Astrophysics of gaseous nebulae and active galactic nuclei*, University Science Books, Sausalito.

[25] Peterson B. M. (1997): *An Introduction to Active Galactic Nuclei*, Cambridge University Press, New York.

[26] Rappaport S., Joss P. C. (1983): *'X-Ray Pulsars in Massive Binary Systems' in Accretion Driven Stellar X-Ray Sources*, Cambridge University Press, Cambridge.

[27] Shakura N. I., Sunyaev R. A. (1973): *Black holes in binary systems. Observational appearance.*, A&A **24** 337-355.

[28] Shapiro S. L., Teukolsky S. A. (1983): *Black Holes, White Dwarfs and Neutron stars*, John Wiley & Sons, New York.

[29] Stella L. (1990): *Measuring black hole mass through variable line profiles from accretion disks*, Nature **344** 747-749.

[30] Trümper J. E., Hasinger G. (2008): *The Universe in X-Rays*, Springer, Berlin.

[31] White N. E., Kallman T., Swank J. H. (1983): *The X-ray absorption spectrum of 4U 1700-37 and its implications for the stellar wind of the companion HD 153919*, ApJ **269** 264-272.

[32] Wood K. S., et al. (1984): *The HEAO A-1 X-ray source catalog*, ApJS **56** 507-649.

[33] Zel'dovich Ya. B., Novikov I. D. (1971): *Relativistic Astrophysics, Vol. 1*, University of Chicago Press, Chicago.